Research Square

Preprints are preliminary reports that have not undergone peer review.
They should not be considered conclusive, used to inform clinical practice,
or referenced by the media as validated information.

Aminocoumarin-based heme oxygenase activity fluorescence probe reveals novel aspects of HO-1 regulation

Joseph Boyle (joseph.boyle@imperial.ac.uk)
Imperial College London https://orcid.org/0000-0002-4337-3320
Derick Chiappo
Imperial College London
Saul Cooper
Imperial College London
Shivani Sinha
Imperial College London
Lunnathaya Tapeng
Imperial College London
Edward Walter
Imperial College London https://orcid.org/0000-0002-1396-3928
Titan Lai
Imperial College London https://orcid.org/0000-0002-9405-1153
Nicholas J. Long
Imperial College London

Article

Keywords:

Posted Date: November 23rd, 2023

DOI: https://doi.org/10.21203/rs.3.rs-3485680/v1

License: This work is licensed under a Creative Commons Attribution 4.0 International License.
Read Full License

Additional Declarations: Yes there is potential Competing Interest. We hold patent WO2022101635-A1 COMPOUNDS FOR THE DETECTION OF HEME OXYGENASE 1 (HO-1) AND METHODS AND USES INVOLVING THE SAME and are seeking licensing arrangements.

Aminocoumarin-based heme oxygenase activity fluorescence probe reveals novel aspects of HO-1 regulation

Derick Chiappo[1†], Saul M. Cooper[2†], Shivani Sinha[1], Lunnathaya Tapeng[1], Edward R. H. Walter[2], Titan Lai[2], Nicholas J. Long[2‡] & Joseph J. Boyle[1‡]

[1] National Lung and Heart Institute, Imperial College London, Hammersmith Hospital, Du Cane Road, London, W12 0NN, UK.

[2] Department of Chemistry, Imperial College London, Molecular Sciences Research Hub, White City Campus, Wood Lane, London, W12 0BZ, UK.

† equal contribution
‡ equal contribution

Corresponding Authors: Joseph J. Boyle (joseph.boyle@imperial.ac.uk)
Nicholas J. Long (n.long@imperial.ac.uk)

Abstract:

Heme oxygenase-1 (HO-1) is crucial for vascular health and heme homeostasis. Whilst protective, HO-1 is increased in numerous cardiovascular diseases, including atherosclerosis. We previously reported a prototype fluorescent probe for HO-1 enzyme activity. Here, we describe the synthesis and biological characterisation of an improved novel red-shifted HO-1 fluorescent probe, AMC-Hem. Its use yielded novel insights into HO-1 regulation in human monocyte-derived macrophages (hMDMs). AMC-Hem measured and imaged real-time HO-1 activity in live cells for the first time. HO-1 activity was concentrated at the outer edge of lysosomes containing phagocytosed erythrocytes. AMC-Hem identified two novel small molecules that regulate HO-1 enzyme activity, by non-transcriptional mechanisms, a new insight into HO-1-regulation. AMC-Hem measured HO-1 enzyme activity in serum from healthy individuals. Therefore, this study demonstrates real-time measurement and visualisation of HO-1 activity with AMC-Hem for the first time and promises to facilitate new insights into its function and clinical relevance.

Main Text

Introduction

Heme oxygenase-1 (HO-1, *HMOX1)* is a key cytoprotective enzyme in the vasculature. HO-1 catalyses the oxidation of heme into biliverdin, ferrous iron, and carbon monoxide. In humans, *HMOX1*-deficiency is lethal in childhood, with death from intravascular occlusion, elevated serum hemin, tissue iron deposition and anaemia [1, 2]. *HMOX1*-deficient mice have a phenotype similar to human disease showing the fundamental importance of the pathway [2, 3]. HO-1 is implicated in the pathogenesis of atherosclerosis, is elevated in atherosclerosis, yet appears to be most likely protective in function, constituting an endogenous brake on disease [4]. That is, HO-1 heals.

Atherosclerosis is the major cause of heart attacks and strokes and is characterised by the build-up of fatty inflamed tissue (plaque) that narrows arteries and eventually destabilises, causing clotting and vascular occlusion [5]. Destabilisation is associated with intraplaque hemorrhage and bleeds within the plaque [5, 6]. The identification of vulnerable plaques is a key component of improved disease management. Intracoronary catheter-based optical imaging has emerged as a diagnostic approach. Various approaches to activity-based fluorescent probes have recently been developed for several enzymes [7].

In atherosclerosis, HO-1 is primarily expressed by a type of inflammatory cell in areas of intraplaque hemorrhage (IPH), termed hemorrhage-associated-macrophage (Mhem) [8]. These comprise human monocyte-derived macrophages (hMDM) specialised for healing of hematomas, tissue blood deposits [4, 9, 10]. HO-1 appears to be atheroprotective as *HMOX1*-deficient mice develop accelerated atherosclerosis with increased inflammation and oxidative stress [11, 12]. This may reflect the key role of hemin-induced HO-1 in hematoma resolution [10].

Previously, we described the development of the first optical imaging probe to report on the activity of HO-1, in an engineered *E. Coli* lysate system expressing recombinant mammalian human HO-1 at extreme levels [13]. The hydroxycoumarin-hemin conjugate (HOC-Hem, Fe–L^1) (**Figure 1A**) was found to "break-apart" regio-selectively at the α-position, forming compound **(1)** (**Figure 1B**). This interrupts the efficient fluorescence resonance energy transfer (FRET) process from its coumarin FRET-donor to the porphyrin FRET-acceptor, causing de-quenching and a *6*-fold increase in coumarin emission intensity. The analogue Fe–L^2 (**Figure 1C**) was not an HO-1 substrate due to the steric inhibition [13].

This current study describes an improved analogue, AMC-Hem (**Figure 1D).** Relative to HOC-Hem, it is slightly red-shifted in the UV spectrum. This has yielded insights into the regulation, intracellular localisation and clinical translation of HO-1. The reagent allowed a far easier and quicker approach to HO-1 measurement than existing protein-based assays. HO-1 activity was imaged in live primary human cells for the first time. It facilitated the insight that HO-1 activity is related to lysosomes and facilitated an improved understanding of HO-1 regulation. It facilitated a 96-well plate-based assay that uncovered another layer of HO-1 regulation. Whilst *HMOX1* was thought to be entirely transcriptionally regulated, this showed a second layer of regulation. It facilitated measurement of HO activity in normal human serum in real time, which opens up possibilities for near-patient testing in hemolytic or hemorrhagic diseases.

Results

Synthesis and photophysical characteristics

We synthesised AMC-Hem, a ferrous-metallated porphyrin derivative functionalised on the α-*meso*-carbon with an aminocoumarin. AMC-Hem was synthesised in a multi-step reaction sequence **(Figure 1E)** analogous to that described for the previous probe HOC-Hem / Fe–L^1 (**Figure 1A**) [13]. An aminocoumarin derivative **(Figure 1E-3)** was selected to slightly red-shift (*circa* 50 nm) the absorbance and emission maxima to facilitate improved detection with only minimal changes to the original **HOC-Hem** structure. The molecular identity of AMC-Hem **(Figure 1E-6)** was confirmed by MALDI mass spectrometry which indicated the presence of the molecular ion peak (**Supplemental Data 1, Figure S19**). Characterisation of novel compounds can be found in Supplemental Data 1.

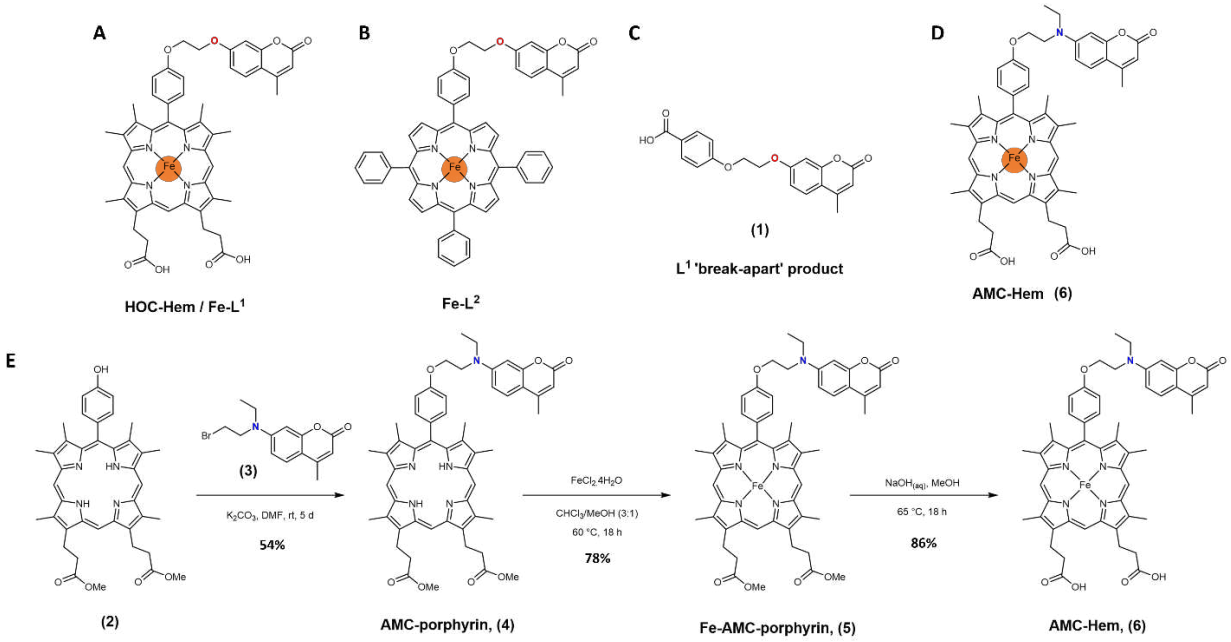

Figure 1: The structure and synthesis of the aminocoumarin derivative AMC-Hem
The structure of Fe-L^1 **(A)**, Fe-L^2 **(B)**, and hydroxycoumarin "break-apart" fluorophore **(C)** as described in our previous work [13]. The structure **(D)** and synthesis scheme of AMC-Hem **(E)**.

The photophysical characterisation of AMC-Hem in PBS buffer (pH = 7.4) and chloroform is shown in **Table 1** and **Table S1** respectively. AMC-Hem displayed an excellent (>99.9%) FRET efficiency in both PBS buffer (pH = 7.4) and chloroform (**Figure S1**), demonstrating a substantial decrease in aminocoumarin fluorescence on conjugation to the porphyrin α-position. The FRET efficiency of >99.9%, was an improvement on the analogous HOC-Hem conjugate and indicated that the red-shifted spectra improved the quenching efficiency. The approximately doubled extinction coefficient observed for the UV band of AMC-Hem relative to HOC-Hem (4.2 vs 2.2 x 10^4 $M^{-1}cm^{-1}$) likely relates to the highly similar absorption wavelength of the porphyrin Soret band to the aminocoumarin absorption at 371 nm (**Figure S3**).

In PBS buffer, aminocoumarin derivative **(3)** displayed a 53 nm and 90 nm red-shift in its absorbance and emission maxima respectively, relative to its HOC analogue. The wavelength maximum of compound **(3)** was selected as the excitation wavelength, due to no significant shift in the wavelength maxima of the coumarin moiety following the formation of the coumarin-porphyrin dyad **(4) (Figure S3)**. Similarly, HOC-porphyrin displayed no significant shift in the wavelength maxima of the coumarin moiety following the formation of the coumarin-porphyrin conjugate [14]. The absorbance spectrum of AMC-Hem is shown in **Figure S3** and is consistent with the findings observed for HOC-Hem (Fe–L^1), albeit with increased extinction coefficient in chloroform (Table S1). We also synthesised aminocoumarin **(9)** in a two-step synthesis to corroborate the photophysics of the emissive 'break-apart' product (**Supplemental Data 1, Figures S6-9**).

	λ_{abs} [nm] (ε / 10^4 $M^{-1}cm^{-1}$)			λ_{em} [nm]	E [%]
	UV	**Soret**	**Q-band**		
Fe-L^1 [b 11]	321 (2.2)	401 (3.0)	[d]	383 [e, f]	99.6
Fe-L^2 [b 11]	320 (1.2)	417 (1.5)	587 (0.8), 629 (0.7)	383 [e, f]	99.4
AMC-Hem [c]	371 (4.1)	[g]	492 (0.6), 634(0.3)	471 [h, f]	99.9
(3)	374 (2.2)	-	-	461	n/a
(9)	374 (0.8)	-	-	460	n/a

Table 1 Photophysical data for AMC-Hem, **(3)** and **(9)** and the hydroxycoumarin analogues Fe–L^1 and Fe–L^2.[a] The structures of **(3)** and **(9)** are found in **Supplementary Data 1, Figures S10 and S18**, respectively. [a] Concentration = 20 μM in PBS buffer (pH = 7.4). [b] λ_{ex}= 320 nm, 298 K. [c] λ_{ex}= 320 nm, 298 K. [d] Broad Q-bands. [e] Residual coumarin emission. [f] No porphyrin emission was observed. [g] Soret band hidden by AMC abs. [h] λ_{ex}= 374 nm, 298 K.

AMC-Hem reveals real-time HO-1 enzyme activity in human inflammatory cells

The HOC-Hem has previously been biologically characterised in a relatively artificial system, based on cell-free enzyme recovered from *E.Coli* engineered for high protein expression and transformed with a recombinant HO-1-expression plasmid [11]. With the AMC-Hem, we opted to study a far more relevant biomedical system. We chose human blood-derived macrophages (hMDM), which are highly representative of pathophysiology [15]. We first assessed the ability of AMC-Hem to detect HO-1 activity in hMDMs in real-time. We stimulated hMDMs with 20 μM hemin with or without 5 μM AMC-Hem for 96 h following pre-incubation with 10 μM OB24 [16]. OB24 is a competitive inhibitor of HO-1 with greater than 50-fold selectivity for HO-1 over HO-2, and an IC50 for HO-1 of 10 μM, the concentration we used in culture [16] [17]. IC50 is the concentration for half-maximal inhibition and is characteristic for inhibitor / enzyme pairs [17].

The cell supernatants were recovered and submitted for fluorescence spectroscopy, which showed an emission peak from 455 and 470 nm, maximal at 465 nm (**Figure 2A**). This closely matched the emission spectrum of the predicted AMC-α-*meso*-carbon breakaway fragment (9) in the same medium (**Figure 2B**). The data for hemin-treated hMDMs with or without pre-treatment with 10 μM OB24 are shown in **Figure 2C**. Stimulation with hemin, which induces *HMOX1* 20-fold at 4 h, stimulated AMC-Hem-related fluorescence. Pre-treatment with 10 μM OB24 significantly reduced the fluorescence signal by 46 ± 12% (**Figure 2C, inset)** – which matched the IC50 (10 μM) OB24 on HO-1 activity. Thus, the fluorescence signal was generated specifically by HO-1 in live hMDM.

As a control we could exclude that OB24-related fluorescence reduction was related to suppressed levels of *HMOX1*, rather than active site blockade. In this experiment, hMDMs were incubated with and without OB24 and with and without hemin for 4 h and *HMOX1* measured by reverse-transcription polymerase chain reaction (RT-qPCR) (**Figure 2D).** Hemin induced *HMOX1* mRNA and protein at 4 h as before [15] . OB24 (10 μM) did not affect *HMOX1* levels either with or without hemin stimulation (**Figure 2D, white and yellow bars)**. Furthermore, AMC-Hem did not affect the expression of *HMOX1* by hMDMs after 4 hours with or without hemin (**Supplemental Data 2 Figure S1B**). Therefore, we concluded that AMC-Hem measures HO-1 activity in live hMDM in real time, representative human inflammatory cells [16].

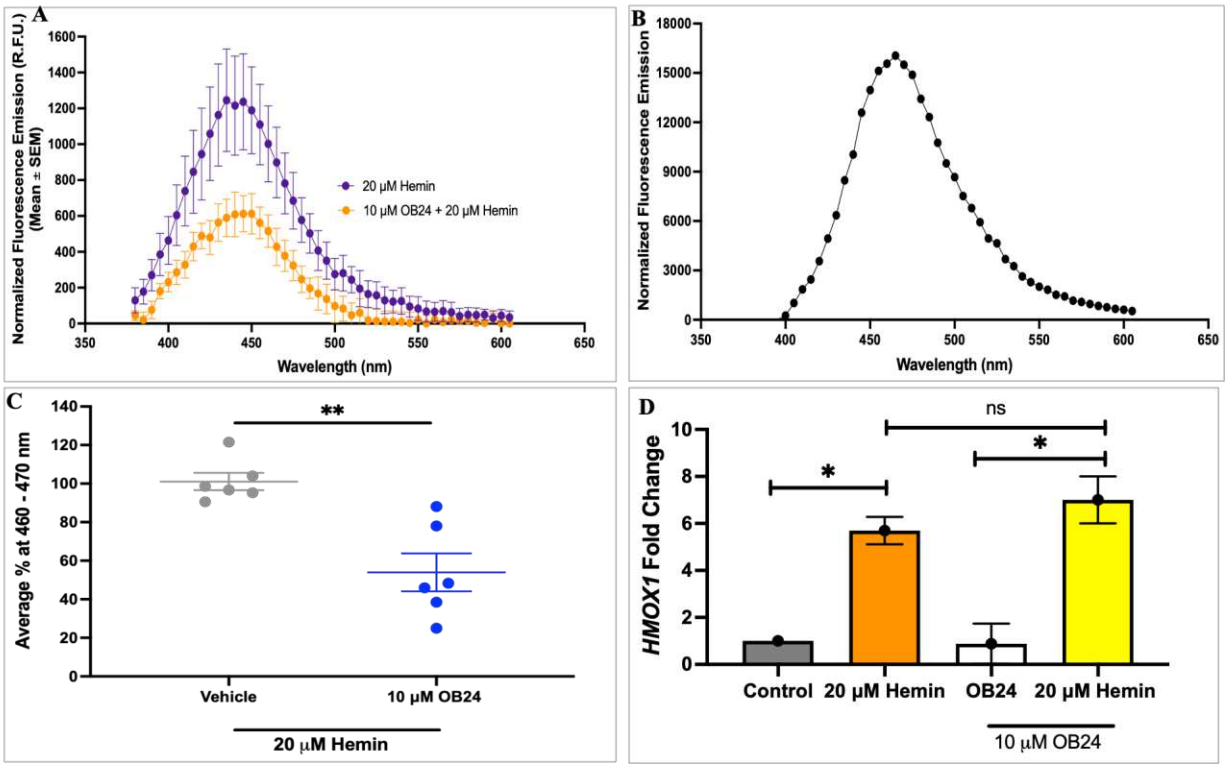

Figure 2: Fe-AMC is catabolised by HO-1 in hMDMs
A) Normalised emission spectrum of cells exposed to 5 µM AMC-Hem with 20 µM hemin with or without 10 µM OB24 (n = 5). **B)** Normalised emission spectrum of 5 µM AMC-Hem "breakaway" in IMDM. **C)** The average percentage value between wavelengths 460 and 470 nm per biological donor. The emission spectrum of cells incubated for 96h with AMC-Hem and hemin with or without OB24 pre-treatment is shown in **Supplemental Data 2 Figure S2A**. **D)** *HMOX1* expression from hMDMs treated for 4 h with 20 µM hemin with or without 10 µM OB24 (n = 5 biological replicate). *p<0.05 vs. Nil, ns = not significant (Kruskal-Wallis Test).

AMC-Hem reveals that HDAC2 regulates HO-1 activity but not levels in hMDM, whilst HDAC3 oppositely regulates HO-1 levels and activity

Improved understanding of the regulation of HO-1 in disease may improve therapeutics. Increasing HO-1 activity may be protective. HO-1 is typically understood to be primarily regulated transcriptionally *i.e.* increasing or decreasing mRNA production from its gene *HMOX1*. However, the methodology for this is labour-intensive, in contrast to the simple addition of AMC-Hem. We, therefore, attempted to use the AMC-Hem probe to assess the relative contribution of different Histone Deacetylases (HDAC) to the transcriptional regulation, as these are targets for multiple drugs in development. Broadly put, histone acetylation is a part of gene activation, so HDAC repress genes, so in turn HDAC-inhibitors (HDACi) activate genes.

We assessed a set of HDACi of overlapping specificity, with HO-1 activity as readout, using AMC-Hem to measure the increased HO-1 activity of hemin-induced *HMOX1*. For pathophysiological relevance, we maintained with hMDMs, which were pre-treated with each HDACi from 20 minutes before hemin to the experiment end, stimulated with hemin and activity read with 5 μM AMC-Hem (96 h). The inhibitor data are shown in **Supplemental Data 2 Table 1**. The inhibitors were added at the IC50 for the most sensitive HDAC isoform. Each had a different pattern of specificities, on hemin-induced HO-1 activity, allowing permutational identification of the HDAC isoform.

The effect of multiple HDACi are summarised in **Figure 3A**. The three HDACis that differentially regulated hemin-induced HO-1 activity were RGFP966, tucidinostat and vorinostat (**Figure 3A**). HO-1 activity was increased by tucidinostat and vorinostat (**Figure 3A**). Tucidinostat preferentially inhibits HDACs 1, 2, 3 and 10 [18]. Vorinostat preferentially inhibits HDAC 1, 2, 3 and 8 [19]. This pointed to HDACs 1, 2, 3 (Class I HDACs) as potential repressors of HO-1 activity.

In contrast, HO-1 activity was suppressed by RGFP966, a selective HDAC3 inhibitor with an IC_{50} of 80 nM and does not inhibit other HDACs up to 15 μM [20]. RGFP966 decreased HO-1 activity by 25 ± 13% (**Figure 3C, inlet).** This was unexpected as HDAC3-deficiency was protective in atherosclerosis via effects on macrophages [21]. Nevertheless, it excluded HDAC3 as the HDAC isoform *repressing* HO-1 activity, leaving either HDAC1 or HDAC2. Therefore, we next tested an HDAC-2-selective inhibitor, santacruzamate (IC_{50}: 0.12 nM) [21, 22]. Pre-incubation with santacruzamate significantly upregulated HO-1 activity by 140 ± 45% compared to hMDMs stimulated with hemin alone (**Figure 3B, inset**). Thus, HDAC-2 was identified as the HDAC isoform repressing HO-1 activity.

HO-1 was understood to be primarily transcriptionally-regulated. We, therefore, anticipated that HDAC2-inibition would increase *HMOX1* transcript levels, whereas HDAC3-inhibition would decrease *HMOX1* transcript levels and tested this, using RT-qPCR which is more labour intensive but addresses the mechanism of regulation.

Unexpectedly, Santacruzamate suppressed hemin-induced *HMOX1* mRNA (**Figure 3D**) although it had increased HO-1 activity. Moreover, RGFP966 increased hemin-induced *HMOX1* mRNA (**Figure 3E**), although it had suppressed activity. These data, therefore, showed an interesting reciprocity between gene activity and enzyme activity of HO-1, and indeed between HDAC2 and HDAC3. A full analysis of the mechanism of non-transcriptional regulation is beyond the scope of the present paper. Notwithstanding, the data show that AMC-Hem can be used relatively easily in a 96-well plate assay to identify pharmacological regulation of HO-1, yielding new potential insights.

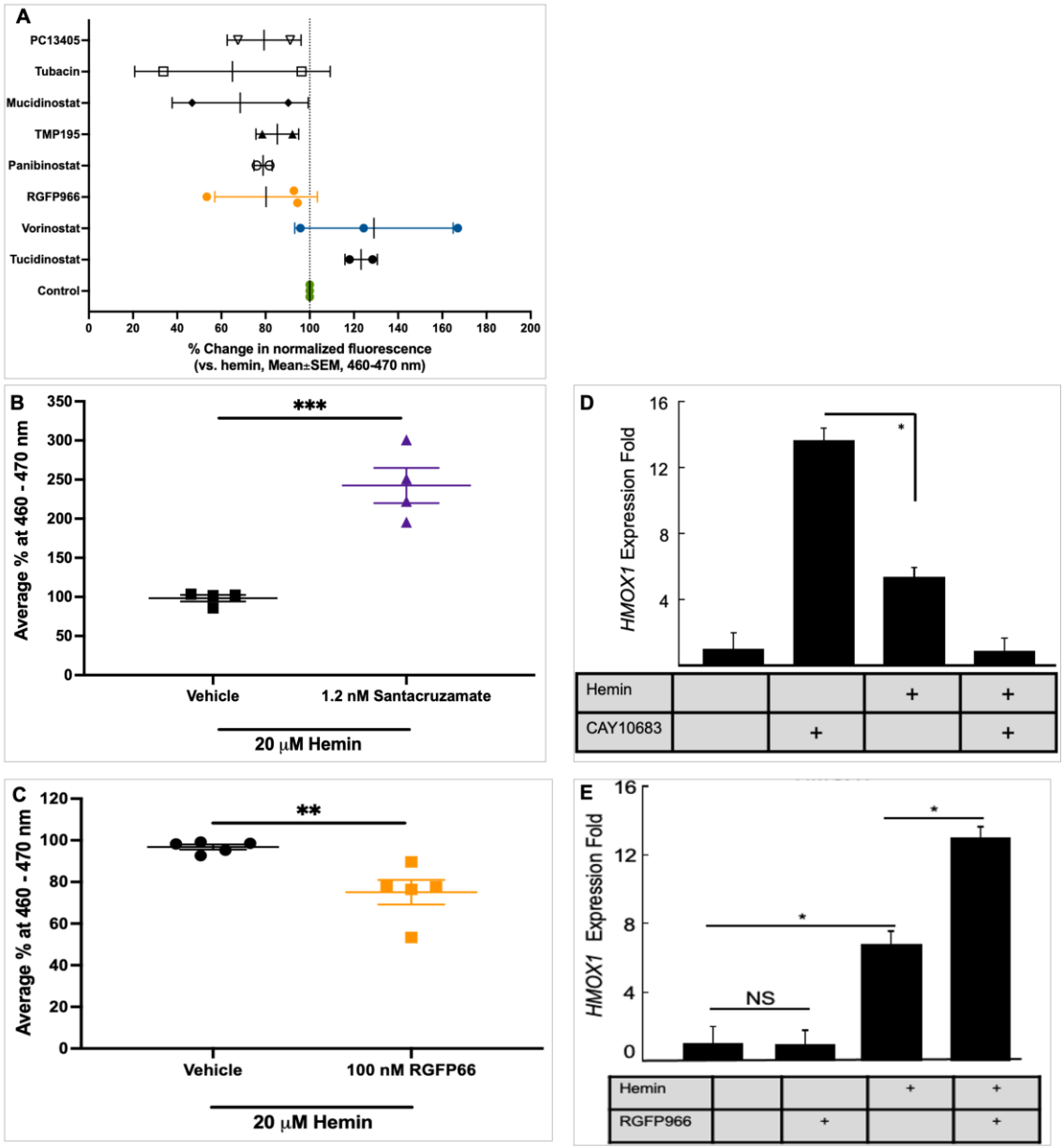

Figure 3: Differential regulation of HMOX1 enzyme activity and expression with inhibition of HDAC2 and HDAC3
(A), Summary of application of AMC-Hem in a high-throughput well assay to identify HDAC inhibitors that differentially regulate HO-1 enzyme activity (n = 2-3 biological replicates as indicated). The HDAC inhibitors, their specificities, and the concentrations used are detailed in the online methods **(**Supplementary Data 2 Table S1**).**

(B) 1.2 nM santacruzamate increases HO-1 activity in hMDMs. Y-axis, % change of santacruzamate-treated and hemin-stimulated cells vs that of hemin-stimulated hMDMs alone. X-axis, treatment, with and without santacruzamate. ***1.2 nM santacruzamate vs. Vehicle, unpaired t-test (n = 4 biological replicates). The emission spectrum at 96 h of cells stimulated with hemin with or without santacruzamate pre-treatment is shown in Supplemental Data 2 Figure S2C.

(C) 100 nM RGFP966 suppresses HO-1 activity in hMDMs. Y-axis, % change of RGFP966-treated and hemin-stimulated cells vs that of hemin-stimulated hMDMs alone. ***100 nM RGFP966 vs. Vehicle, unpaired t-test (n = 5). The emission spectrum at 96 h of cells stimulated with hemin with or without RGFP966 pre-treatment is shown in Supplemental Data 2 Figure S2B.

(D) Santacruzamate suppresses hemin-induced *HMOX1* expression. X-axis, treatment with Santacruzamate (CAY10683) and hemin as indicated in the table. Y-axis, *HMOX1* gene levels by RT-qPCR (Fold increase). n= 6 healthy donors, *p<0.05, repeated measures ANOVA with SNK post-test for indicated comparison.
(E) RGFP966 increases hemin-induced *HMOX1* expression. X-axis, treatment with RGFP966 and hemin as indicated in the table. Y-axis, *HMOX1* gene levels by RT-qPCR (Fold increase), n= 9 healthy donors, *p<0.05, repeated measures ANOVA with SNK post-test for indicated comparisons

AMC-Hem demonstrates HO-1 activity at the junction of the lysosomes

HO-1 operates not alone as an enzyme but in a complex with other proteins and requires access to NADPH cofactor and substrate [23–25].Thus, cell location and partner proteins are potential key regulators of HO-1-activity independent of *HMOX1* transcription. One of the ways that HO-1 could be post-transcriptionally regulated is via regulation of cofactor supply. We therefore assessed the cell location of AMC-Hem signal. We carried these experiments out in hMDM for pathophysiological relevance. We and others have shown that hemorrhage-related debris e.g. erythrocytes, is trafficked into lysosomes following phagocytosis by hMDMs [4, 26]. Moreover, we previously found overlap between staining for HO-1 and CD68 (a lysosomal protein). Therefore, we next tested whether AMC-Hem is trafficked into lysosomes and how HO-1 activity relates to AMC-Hem-containing lysosomes. Lysosomes were visualised in live hMDMs by staining with lysotracker red, a cell-permeable hydrophobic-basic fluorophore that in acidic compartments becomes protonated, charged, and retained [27].

Figures 4A and B show images of hMDMs incubated with 10 μM AMC-Hem for 96 h, or control hMDMs. Intracellular blue fluorescence was increased in AMC-Hem-treated compared to control hMDMs. These showed an apparent gradient, consistent with diffusion from the location of phagocytosed probe (**Figure 4B, white arrows**). This AMC-Hem probe signal co-localised with the lysotracker red fluorescence (**Figure 4B, white arrows).** In the control hMDMs, the distribution of lysosomes is diffuse in the cytoplasm (**Figure 4A, yellow arrows**). A representative image of hMDMs incubated with 20 μM hemin for 96 h is found in **Supplementary Data 2 Figure S3**.

We next quantified the AMC-Hem-related fluorescence (using AMC-Hem-untreated macrophages as a control). hMDMs incubated with 10 μM AMC-Hem had increased

intracellular fluorescence compared to cell autofluorescence in control hMDMs (**Figure 4C)**. hMDMs stimulated with 20 μM hemin with 10 μM AMC-Hem generated significantly more fluorescence than those incubated with 10 μM AMC-Hem alone (**Supplementary Data 2 Figure S1B**), consistent with HO-1 being hemin-inducible.

We next addressed in more detail the co-localisation between HO-1 activity and lysosomes by quantifying it (**Online methods Figure 1**). We compared fluorescence intensity in the AMC-Hem (blue) and lysotracker (red) channels along a radius from the geometric centre of the lysosome. As might be expected, lysosomal marker intensity decreased with distance away from the lysosome centre. AMC-Hem fluorescence increased with distance away from the lysosome centre and was maximal at the lysosome / cytosol boundary (**Figure 4D)**. Thus, HO-1 activity appeared to localise to the junction of lysosome and cytosol, or external lysosomal membrane, with the limits of optical resolution. This imaged, for the first time, HO-1 enzyme activity in human primary cells.

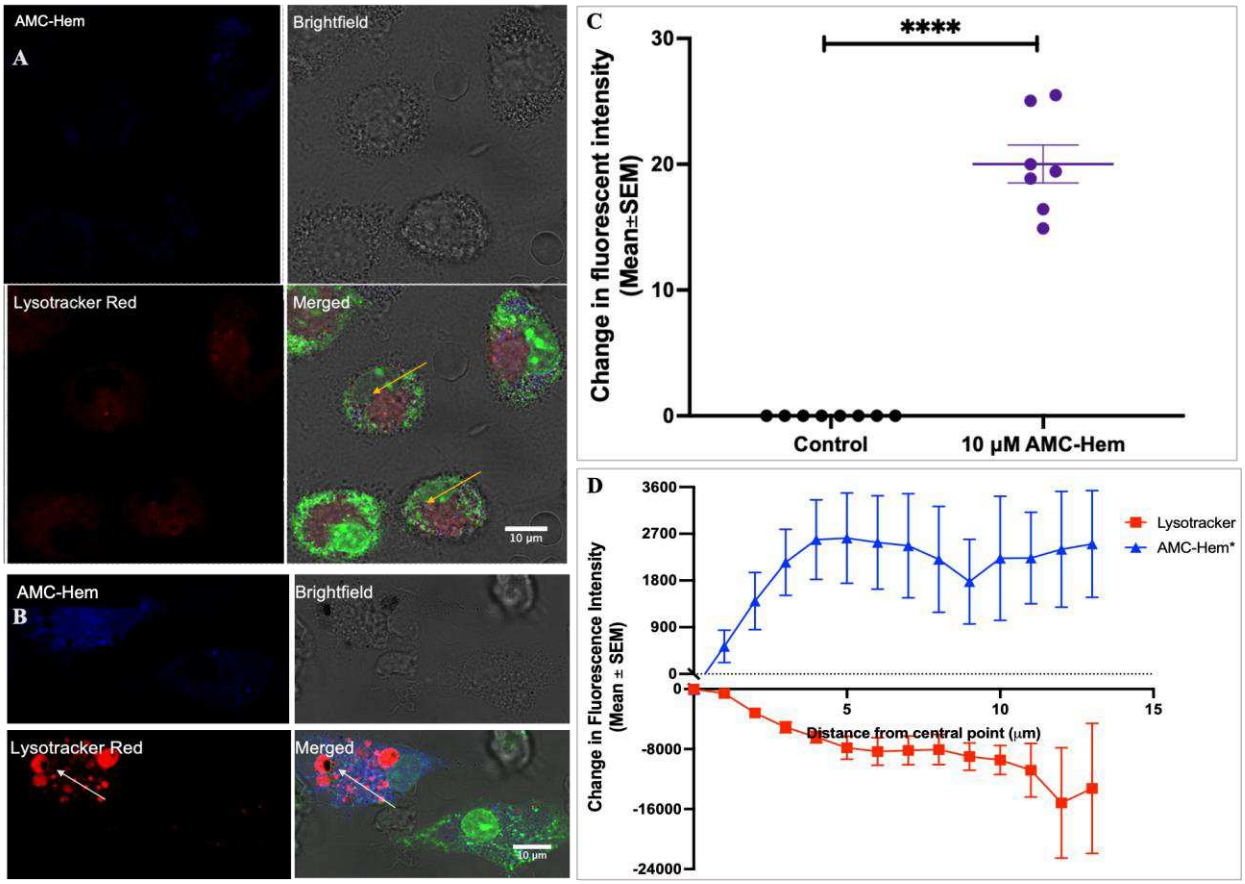

Figure 4: Intracellular visualisation and localisation of HO-1 activity with AMC-Hem

Figure 4A colours are Grey - brightfield DIC; red -lysotracker red; green - DNA, blue - AMC-Hem / NADPH. Figure 4A, B were taken at matched intensity, sensitivity, brightness and contrast settings and show faint NAPDH fluorescence (yellow arrow, A) and more intense blue fluorescence with addition of AMC-Hem (white arrow, B). In B, white arrow, the AMC-Hem related fluorescence is at the edge of a lysosome that contains a deposit of AMC-hem.
Representative image of control hMDMs **(A)** and hMDM incubated with 10 μM AMC-Hem for 96 h **(B). C)** Change in fluorescence in the AMC-Hem channel in control hMDMs vs hMDMs incubated with 10 μM AMC-Hem (n = 8). Each dot represents a grand mean of 20 cells from each biological replicate. *** 10 μM AMC-Hem vs. Control, unpaired T-test. **D)** Change in pixel fluorescence in two channels (Fe-AMC and Lysotracker) from the centre of a lysosome, as identified by Lysotracker (n = 6). *AMC-Hem values were transformed by multiplying the real value by 100.

Detecting HO-1 activity during erythrophagocytosis

Having validated AMC-Hem fluorescence, we next assessed its likely pathophysiological relevance, in an erythrophagocytosis model. Erythrophagocytosis comprises macrophage eating erythrocytes, and occurs in healing tissue hemorrhages, some inflammatory pathophysiologies, and normal spleen [8, 28]. In atherosclerosis, erythrophagocytosis is related to oxidative damage to erythrocyte and intraplaque hemorrhage [28, 29]. Moreover, HO-1 is a crucial protectant, as erythrophagocytosis kills *Hmox1*-deficient murine macrophages, but not controls [30]. Therefore, AMC-Hem was investigated in hMDM-mediated erythrophagocytosis.

We showed that Ru-PPIX tracers with metalloporphyrin analogues could be loaded into erythrocytes [10]. We adapted the approach to load AMC-Hem into oxidised erythrocytes, which already contain substantial amounts of heme [10]. These were added to hMDM, which were serially analysed by fluorescence spectroscopy over 96 h (**Figure 5A).** A graph of AMC-Hem-dependent fluorescence with time showed that it was maximal by 24 h and maintained for 72 h (**Figure 5A**). The inlet in **Figure 5A** demonstrates a slight shift in peak emission wavelength from 430 to 450 nm in AMC-Hem-loaded OxRBCs stimulated macrophages compared to those exposed to AMC-Hem. This was significantly earlier than free 5 μM AMC-Hem (24 h *cf* 96 h). The more rapid activity may relate to the more physiological presentation of AMC-Hem.

Next, the hMDM were examined by fluorescence confocal microscopy **(Figures 5C** and **5D).** This showed that macrophages have phagocytosed erythrocytes within lysosomes. hMDMS stimulated with AMC-Hem-loaded OxRBC displayed overlapping blue AMC-

Hem-related fluorescence and lysotracker red in red blood-like shapes (**Figure 5C, white arrows).** Other staining patterns observed are shown in **Supplementary Data 2, Figures S4A and B.** These staining patterns differ from free probe exposed cells where blue fluorescence emanates from phagocytised free probe. This imaged, for the first time, HO-1 activity in macrophages actively engaged in erythrophagocytosis and detoxification of erythrocyte contents.

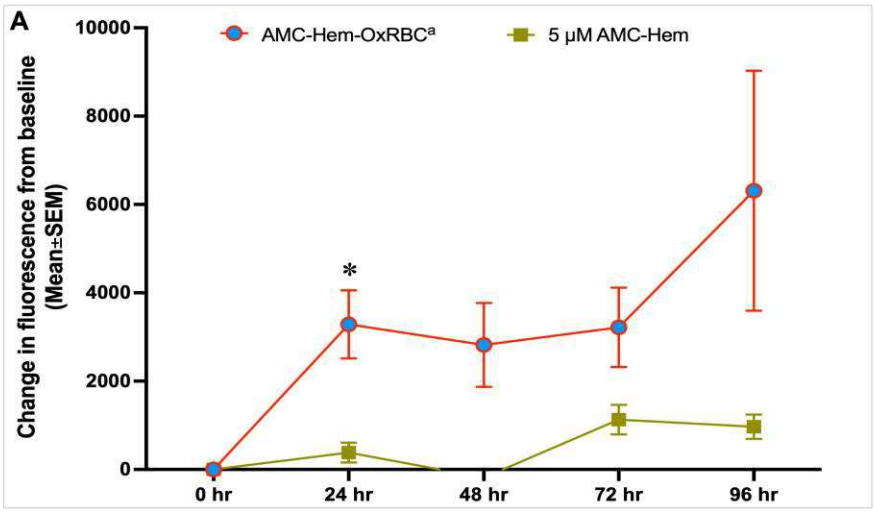

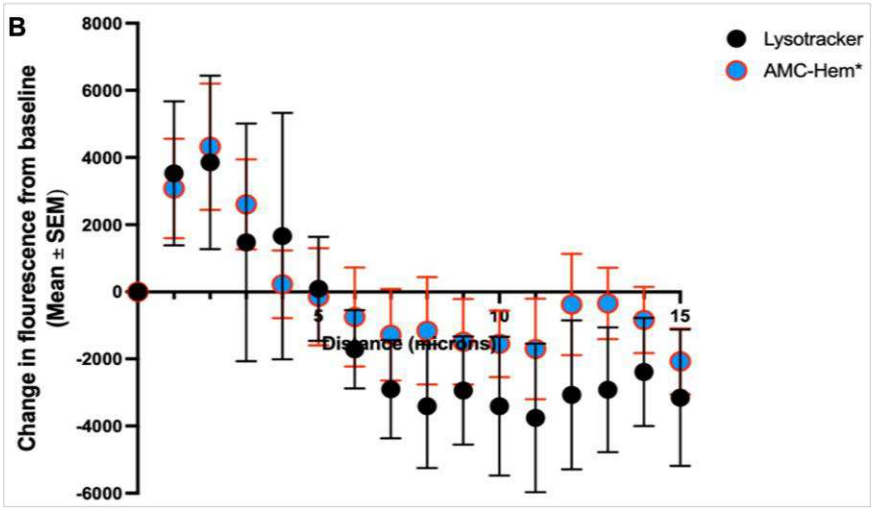

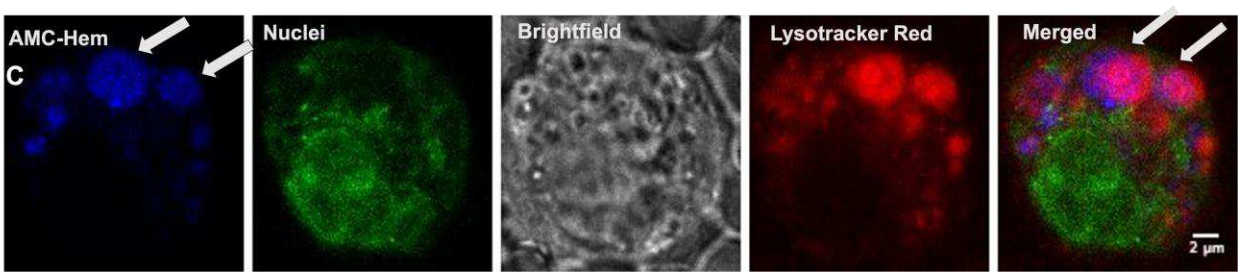

Figure 5: Using AMC-Hem to study HO-1 activity during EP
Time course of AMC-Hem fluorescence generated by hMDMs incubated with 5 μM AMC-Hem (green squares) or stimulated with AMC-Hem-OxRBC (red, blue-filled circles) (**A**). *p <0.05, 24 h vs. 0 h repeated measures one-way ANOVA with Holm-Sidak post-hoc correction. [a] Fluorescence was normalised against that from hMDMs stimulated with unloaded oxidised erythrocytes. The emission spectrum after 96h of incubation with AMC-Hem loaded OxRBCs is shown in **Supplemental Data 2 Figure S2D**. **B)** Change in pixel fluorescence in two channels (AMC-Hem and Lysotracker) from the centre of a lysosome, as identified by Lysotracker (n = 6). *AMC-Hem values were transformed by multiplying the real value by 1000. Representative images of the cell used in the analysis in **Figure 5B** are shown in **Figure 5C**. The contrast in the image was enhanced using ImageJ's auto function under Brightness and Contrast.

HO-1 and its co-enzymes, cytochrome P450 terminal reductase and Glucose-6-phosphate dehydrogenase, are recruited to the phagolysosome

Given the overlapping lysosomal and AMC-Hem-related fluorescence, we next used immunofluorescence on fixed hMDMs to investigate the location of HO-1 relative to lysosomal marker, lysosome-associated membrane protein 1 (LAMP-1), and two other proteins involved in HO-1 activity, cytochrome P450 oxidoreductase (CYP450POR) [31] and glucose-6-phosphate dehydrogenase (G6PD) [32, 33]. We stained for G6PD as macrophages have increased pentose phosphate pathway activity in response to heme, particularly via G6PD[32].

Supplementary Data 2 Figures S6A and B show representative hMDM co-stained for HO-1 and G6PD, or LAMP-1, a lysosomal marker [34, 35]. LAMP-1 appeared cytoplasmic and concentrated around the OxRBC on erythrophagocytosis. HO-1 / LAMP-1 co-staining revealed specific co-localisation of HO-1 and LAMP-1 around the phagocytic cup. Similarly, G6PD and HO-1 co-localised around the phagocytic cup. **Supplementary Data 2 Figures S7A and B** show representative hMDM co-stained for Cytochrome P450 terminal reductase (CYP450POR) and LAMP-1 or G6PD, respectively. Like HO-1, NADPH terminal reductase and G6PD both co-localised with LAMP-1 staining around the phagocytosed OxRBC. Therefore, HO-1 is co-localized to phagolysosomes containing OxRBCs, with G6PD, which produces it cofactor NADPH, and CYP450POR which transfers electrons from NADPH to HO-1. These localisations correspond closely to HO-1 activity with AMC-Hem and help explain its full activity adjacent to phagolysosomal OxRBCs.

AMC-Hem enables rapid quantification of serum HO-1

Patients with intracranial hemorrhage develop elevated serum HO-1 [36]. Similarly, patients with coronary artery disease have increased HO-1, and patients with unstable coronary artery disease characterised by thrombus and intraplaque hemorrhage, have levels that are elevated again [37]. Thus, HO-1 activity in macrophages engaged in erythrophagocytosis may become reflected in levels in the systemic circulation. Notably, these protein-based measurements of HO-1 are labour-intensive. We, therefore, assessed the ability of AMC-Hem to measure HO-1 in serum, as a measure of erythrophagocytosis in humans and potentially patients.

We began by adapting our previous measurement protocol (200 μM HOC-Hem with 1 mM NADPH measuring activity in lysates of HO-1-transformed *E. coli* [13]. We adapted this for serum by incubating 100% serum with 0.2 mM NADPH and 5 μM AMC-Hem. The results are shown in **Figure 6A, which shows weak and variable fluorescence**, with a suggestion of signal at 24 h. Therefore, the assay was further optimised. **Supplemental Data 2 Figure S5** summarises the requirements for HO-1 activity, including a continuous supply of NADPH via G6PD [32, 33] and CYP450POR to generate a free electron for HO-1 [31].

Results with the optimised assay conditions are shown in **Figure 6B.** Peak HO-1 activity occurred far earlier (125 minutes) and plateaued for the remaining assay time (**Figure 6B**) and was less variable than before (optimised: 311.3 ± 110.8 (CV: 35.6%), initial 329.6 ± 600.2 (CV: 182.1%), Mean ± SEM). We next measured the HO activity in the 6 healthy control sera at 125 minutes, which showed fluorescence readings = 4.7 ± 1.1 R.F.U. (Mean ± SEM). HO-1 was measured in the same sera by ELISA. This indicated that HO-1 was indeed present in the healthy sera, at levels similar to those previously reported [38, 39]. Using the protein estimations to calculate the turnover number, we found 45.9 ± 13.5 min^{-1}, which is broadly similar to those expected for HO-1 (on hemin). No significant correlation was observed between serum HO-1 levels and enzyme activity at 125 minutes (**Figure 6C**). Therefore, AMC-Hem may measure low levels of serum HO-1, and does so in a more rapid and simple assay than those previously used.

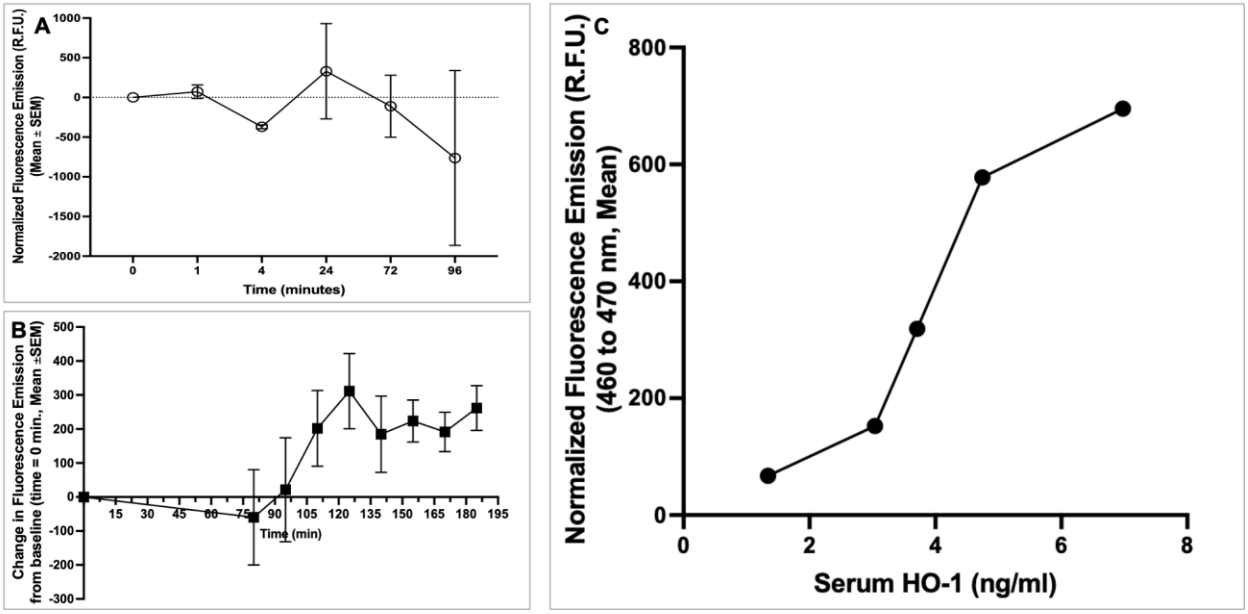

Figure 6: Serum HO-1 activity in pre- and post-optimisation master mixes.

Time course of HO-1 activity pre**- (A, n = 4)** and post-assay buffer optimisation **(B)** with AMC-Hem. **B)** After optimisation, peak serum HO-1 serum activity occurs at 125 minutes (12x faster) amongst serum from six healthy controls. Data points in the first 60 minutes were removed as this time represents the various reagents equilibrating in solution. The full-time course is shown in **Supplementary Data 2 Figure S6A**. **C)** The relationship between serum HO-1 (ng/ml) and activity, as measured by normalized fluorescence. at 125 minutes.

Discussion

This study describes the synthesis and use of an improved fluorescent probe for HO-1 with an emission peak red-shifted from the published prototype (from 380 nm to 465 nm). This enables numerous biomedical applications and has started to yield new insights into HO-1 intracellular localisation, activity and regulation.

Our previous work with AMC-Hem established proof that it may detect HO-1 activity in a highly artificial synthetic system [13]. However, the applicability of HOC-Hem is limited, given its excitation and emission in the UV range. Filters or lasers appropriate for HOC-Hem are not present in most biomedical fluorescence instruments, and may not even be close to optimal wavelengths [40, 41]. Instruments aside, the UV excitation and emission would be photodamaging. AMC-Hem is more applicable to biomedical questions as it emits light at 420-520 nm (blue) and is excitable over 350-410 nm (very near-UV to violet), so is compatible with lasers with 395 or 415 nm lines [40, 41].

AMC-Hem was validated as a specific measure of HO-activity, almost certainly principally HO-1, by inhibition with OB24, known as a highly selective competitive HO-1 inhibitor (IC_{50}: 1.9 ± 0.2 μM) [16] [17]. OB24 was characterised as having a concentration for half-maximal inhibition (IC50) of HO-1 of 10 μM and 50-fold selectivity for HO-1 over HO-2 [16] [17]. As OB24 reduced AMC-Hem fluorescence in hMDM by approximately 50% at 10 μM, it principally reflects HO-1. This importantly excludes a significant contribution of non-specific lysis [16, 17]. HO-1 is the principal isoform expressed in hemin-stimulated or erythrophagocytic hMDM [42] [15, 43]. So activity with HO-2 is possible but likely not material to these uses.

This study shows for the first time HO-1 activity in real-time in representative mammalian cells. Moreover, we studied erythrophagocytosis, a key disease process, in hMDM, which are derived from circulating phagocytes of healthy human donors and were unmodified. HO-1 is usually thought of as a cytosolic soluble enzyme without any given distribution. However, a small number of more detailed papers revealed membrane-tethering, possibly on the endoplasmic reticulum and possible coupling to enzymes CYP450POR and Biliverdin Reductase (BVR) [44–46]. Intriguingly, we showed co-localisation of activity to

the periphery of the lysosome, or the cytoplasm immediately adjacent to the lysosome, this distinction being limited by optical resolution. Consistent with this, HO-1 protein appeared to be co-localised with key enzymes such as G6PD, CYP450POR and BVR. More precise estimates will require super-resolution (which will depend on a more red-shifted dye) or cryo-immuno-electron (Cryo-EM) microscopy. Thus HO-1 activity corresponds to the edge of OxRBC phagolysosomes, most likely due to co-requirements for CYP450POR, BVR, substrate and G6PD / NADPH cofactor. The raises the possibility of a super-complex that assembles on phagolysosomes and actively shields the cell interior from its toxic contents.

The erythrocytes used in these experiments had been made good phagocytic targets by a brief incubation with hydrogen peroxide. This oxidises surface lipids rendering them macrophage scavenger receptor ligands, and is highly pathophysiologically relevant [47]. Interestingly, HO-1 activity developed far more quickly when the probe was delivered in erythrocytes. It seems likely that the more rapid response reflects the more pathophysiologically representative stimulus, possibly because mammalian macrophages are adapted to be able to heal tissue hemorrhage.

AMC-Hem carries multiple advantages over more traditional methods for HO-1 measurement, For example, Bories et al. [32] revealed the co-regulation of HO-1 with its cofactor supply system, the pentose phosphate shunt, and carried out HO-1 assays by lysing the cells precluding serial measurements [32]. Notably, the rate of heme degradation was slow, over days. Classical methods are also destructive, including incubation of hemin with cell lysate and an NADPH generator system, with extraction and semi-purification of bilirubin for measurement [23–25]. AMC-Hem can measure HO-1 activity continuously in intact cells with a single addition, with use operationally similar to widely-used fluorescent probes for reactive oxygen species [48].

AMC-Hem facilitated an improved definition of the roles of specific HDAC isoforms in regulating HO-1 activity. HDAC2 and HDAC3 inhibitors had reciprocal and opposing effects on HO-1 enzyme activity and *HMOX1* expression. HDAC3 inhibition increased expression but reduced activity, whilst HDAC2 inhibition increased activity but reduced

expression. This disconnect, indeed reciprocity, between *HMOX1* gene expression and HO-1 activity levels is intriguing and appears not be described before. Follow-up is under way and a full dissection is beyond the scope of the current paper. It seems unlikely this effect would have been discovered without the Hem-AMC probe. In atherosclerosis, HDAC3-deficiency in murine myeloid cells is protective [21]. Similarly, HDAC2 inhibition may be anti-inflammatory [49] [50]. Thus both drugs may be protective and inhibiting both enzymes may be synergistic. Further work may establish the mechanism by which HDAC2 inhibition increases HO-1 activity. Regulation of the pentose-phosphate shunt, or the lysosomal colocalisation we here describe are possible hypotheses.

AMC-Hem was investigated as an easy measure of serum HO-1 activity, as this is an area of unmet clinical need. HO-1 may form an important cardiovascular biomarker as HO-1 levels are elevated in unstable coronary artery disease [37]. The approach may have enormous potential in Sickle Cell Disease, an area of profound unmet need. Evaluating the degree of hemolysis during vaso-occlusive crisis (VOC) is a particular challenge due to chronic hemolysis [51]. As the AMC-Hem data showed detectable activity in approximately 1-2 h in 10 µL of sera from healthy volunteers, who would have low HO-1, its detection is likely to be facile in hemolysis.

Moreover, the approach is easily extendable to HO-1 in other biological fluids, including plasma, wound fluids, CSF, and potentially blood itself. HO-1 activity in cell or tissue lysates is indirectly assessed by bilirubin levels [33, 52]. Indeed, so-called xanthochromia has been a clinical hallmark of intracranial hemorrhage. AMC-Hem detected serum measuring HO-1 activity using a facile assay and short time (1-2 h), opening the door to its development in point-of-care (POC) testing. This approach is promising for rapid detection of elevated HO-1 in hemolytic diseases.

We note recent work in which a red-fluorescent probe was attached to a hemin-porphyrin ring via the propionic acid residues [53]. We note both the linkage type (amide) and location to the propionic acid groups which crucially do not enter the enzyme pocket proper and are essentially uninvolved in catalysis of hemin. This molecule's validation as an HO-activity-reporter depended on ZnPPIX, which has a very intense and broad

absorption so would block emission relatively non-selectively. Nevertheless, the approach is interesting and we await further developments.

We designed the HOC-Hem and AMC-Hem probes to act as HO substrates. That is, fluorescence de-quenching is necessarily linked to catalysis by the targeted enzyme, with release of the α-*meso*-carbon. This is akin to FRET-dequenching in peptide, protein and oligonucleotide fluorescence probes for proteases and nucleases [25, 54–56]. We cannot find a previous instance in which this approach has been taken with an endogenous small molecule metabolite. This may relate to the synthetic challenges in the work and the enormous skill required in the synthesis. Given this proof of concept and clear utility, it may in the future be possible to take a similar approach with other small molecules.

In summary, we previously described HOC-Hem, a prototype fluorescence turn-on break-apart reporter for HO activity. HOC-Hem was UV-excited, UV-emissive, and was only validated in lysates of bacteria engineered to express extreme levels of HO-1. AMC-Hem is an improved, red-shifted HO-1 “break-apart” FRET probe that we applied to pathophysiologically-relevant questions, initiating new insights into the subcellular localisation of HO-1 activity and its non-transcriptional regulation by HDACs, a novel class of drug target. It enables HO-1 measurement in small amounts of sera from healthy volunteers in a timescale appropriate for near-patient testing and monitoring. A major advantage of this new probe is its ease of use.

Online Methods

General Procedures

All commercially available reagents were used as received from suppliers without further purification. Solvents used were laboratory grade. Anhydrous solvents were obtained from departmental solvent towers and stored over 3 Å molecular sieves. Moisture-sensitive reactions were carried out by Schlenk-line techniques, under an inert atmosphere of nitrogen. Thin-layer and column chromatography was performed on silica (Merk Art 5554) and visualised under UV radiation. ^{1}H (400 MHz) and ^{13}C{^{1}H} (101 MHz) NMR spectra were recorded on a Bruker AV-400 spectrometer, Imperial College London at 298 K. Chemical shifts are reported in parts per million (ppm), and referenced to the solvent. Coupling constants are reported in Hertz (Hz) Peak multiplicities are abbreviated as s = singlet, m = multiple, d = doublet, t = triplet, q = quartet, dd = doublet of doublet and br = broad. Mass spectrometry analysis (ESI and MALDI-MS) was conducted by the Mass Spectrometry Service, Imperial College London, unless stated otherwise. Flash silica column chromatography was performed on a Biotage Isolera Prime advanced automated flash purification unit using Sfär Duo or Sfär C-18 Duo cartridges.

Absorption spectroscopy

UV-Visible absorption spectra were measured using an Agilent Technologies Cary 60 spectrophotometrer operating with WinUV software. The sample was held in a quartz cuvette with a path length of 1 cm. Absorption spectra were recorded against a baseline of pure solvent in an optically matched cuvette with a scan rate of 600 nm / min and a data interval of 1.0 nm. Extinction coefficients were calculated from the Beer Lambert Law (**Equation 1**).

$$A = \varepsilon c l \qquad \textbf{Eq 1.}$$

Where A = the absorbance at a particular wavelength, ε is the extinction coefficient, c is the concentration and l is the path length (width of the quartz cuvette, 1 cm).

Fluorescence spectroscopy

Emission and excitation spectra were acquired on an Agilent Technologies Carry Eclipse fluorescence spectrophotometer, in quartz cuvettes with a path length of 1 cm. Emission and excitation spectra were collected with a scan rate of 120.0 nm / min, a delay interval of 1.0 nm and band-passes of 5 nm. FRET efficiency (E) was calculated according to **Equation 2**.

$$E\,[\%] = 1 - \left(\frac{A_D}{A_{DA}} x \frac{E_{DA}}{E_D}\right) x\, 100 \qquad \textbf{Eq 2.}$$

Where E is the FRET efficiency, A_D and E_D is the absorbance and the emission of the donor fluorophore respectively, and A_{DA} and E_{DA} are the absorbance and emission of the donor fluorophore in the presence of the acceptor. Porphyrin emission and excitation spectra after excitation at the coumarin donor fluorophore were recorded using a 415 nm filter to remove $2\lambda_{ex}$ light from the fluorescence emission and $\frac{\lambda_{em}}{2}$ from the excitation spectrum.

Quantum yields

The fluorescence quantum yield of **(9)** was determined relative to 7-diethylamino-4-methylcoumarin (ϕ_{374} = 0.46)[13] in methanol. Solutions of the reference and the sample were prepared so that the absorbance intensity at 374 nm was 0.1. All measurements were recorded under aerated conditions at room temperature. Absorbance and emission spectrum were run consecutively with identical instrumentation parameters. The quantum yield was calculated from **Equation 3**.

$$\emptyset_a = \left(\frac{I_a}{I_b}\right) x \left(\frac{A_b}{A_a}\right) x \left(\frac{n_a}{n_b}\right)^2 x\, \emptyset_b \qquad \textbf{Eq 3.}$$

Where ∅ is the quantum yield, I is the integrated intensity of the emission spectrum, A is the absorbance at the excitation wavelength and n is the refractive index of the solvent. ‘a’ refers to the sample, and ‘b’ refers to the standard.

pH measurements

Measurements were recorded using a Jenway 3510 pH meter in combination with a Jenway 924 005 pH electrode. Before each independent titration, the pH probe was calibrated using pH 4, 7 and 10 buffer solutions. Aqueous solutions containing Tris (25 mM) and NaCl (150 mM) were made up at different physiologically relevant pH values, and the pH of each solution was confirmed following the addition of **(7)**, **(8)** or **(9).**

Compound synthesis

Compounds (**2**) [13] and (**3**) [57] were prepared according to procedures from the literature.

Dimethyl 3,3'-(10-(4-(2-(ethyl(4-methyl-2-oxo-2*H*-chromen-7-yl)amino)ethoxy) phenyl)-3,7,8,12,13,17-hexamethylporphyrin-2,18-diyl)dipropionate, **AMC-porphyrin (4)**.

Procedure adapted from Long and co-workers [13].

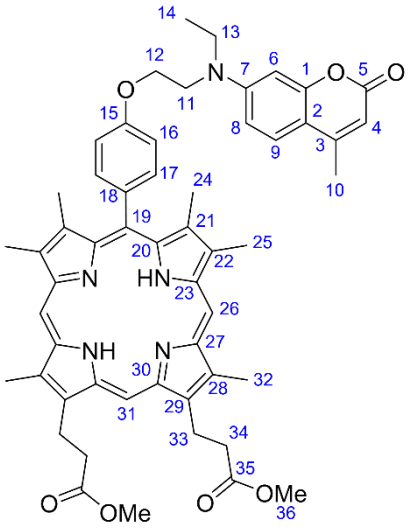

Anhydrous K_2CO_3 (220.4 mg, 1.59 mmol) was added to a solution of **(2)** (78.3 mg, 0.12 mmol) and **(3)** (75.9 mg, 0.25 mmol) in anhydrous DMF (6.5 mL). The reaction was stirred at room temperature for 1 d under an inert atmosphere of nitrogen with protection from light before adding further **(3)** 37.3 mg and K_2CO_3 (73.2 mg). The reaction mixture was stirred for 4 d under nitrogen. The solvent was removed under reduced pressure to form a dark brown residue. Purification by silica gel column chromatography (gradient 100 % CH_2Cl_2 to 99 % CH_2Cl_2 / 1 % MeOH) formed the title compound as a dark red solid (57.1 mg, 54 %). ^{1}H NMR (400 MHz, $CDCl_3$): δ 10.14 (s, 2 H, H^{26}), 9.94 (s, 1 H, H^{31}), 7.80 (d, 2 H, J = 8.3 Hz, H^{17}), 7.45 (d, 1 H, J = 8.8 Hz, H^{9}), 7.13 (d, 2 H, J = 8.3 Hz, H^{16}), 6.76 (dd, 1 H, J_1 = 8.9 Hz, J_2 = 2.5 Hz, H^{8}), 6.72 (d, 1 H, J = 2.5 Hz, H^{6}), 6.02 (d, 1 H, J = 1.1 Hz, H^{4}), 4.39 (t, 4 H, J = 7.8 Hz, H^{34}), 4.34 (t, 2H, J = 5.7 Hz, H^{14}), 3.91 (t, 2 H, J = 5.7 Hz, H^{13}), 3.68 (q, 2H, J = 6.9 Hz, H^{11}), 3.68 (s, 6H, H^{36}), 3.63 (s, 6H, H^{24} or H^{25}), 3.51 (s, 6 H, H^{24} or H^{25}), 3.30 (t, 4 H, J = 7.8 Hz, H^{33}), 2.43 (s, 6 H, H^{32}), 2.35 (d, 3 H, J = 1.1 Hz, H^{10}), 1.35 (t, 3 H, J = 6.9 Hz, H^{12}), - 3.31 (s, br, 1 H, NH), - 3.32 (s, br, 1 H, NH); ^{13}C {^{1}H} (101 MHz, $CDCl_3$) 173.7, 162.2, 158.9, 156.1, 152.9, 150.8, 145.2, 145.0, 143.6, 143.1, 138.2, 137.9, 137.2, 137.0, 135.5, 134.0, 125.8, 118.6, 113.6, 109.9, 109.5, 108.8, 98.4, 96.9, 95.5, 65.5, 51.9, 50.0, 46.2, 37.0, 22.0, 18.6, 15.3, 12.3, 12.3, 11.9; HRMS (*m/z*): $[M+H]^+$ calcd. for $C_{54}H_{58}N_5O_7$, 888.4336, found 888.4341; UV-Vis ($CHCl_3$): λ_{max} / nm (ε / $M^{-1}cm^{-1}$) 406 (176050), 504 (14123), 538 (6376), 572 (6366), 625 (2359).

Iron (II) dimethyl 3,3'-(10-(4-(2-(ethyl(4-methyl-2-oxo-2*H*-chromen-7-yl)amino)ethoxy) phenyl)-3,7,8,12,13,17-hexamethylporphyrin-2,18-diyl)dipropionate, **AMC-Hemporphyrin (5)**

Procedure adapted from Long and co-workers [13].

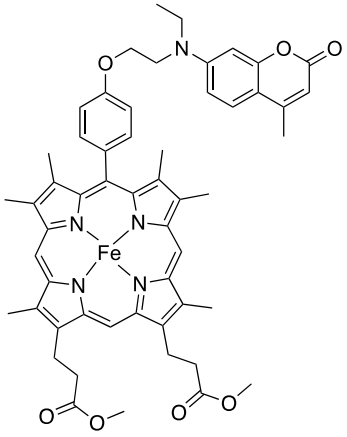

$FeCl_2.4H_2O$ (81.5 mg, 0.41 mmol), sodium hydrogen carbonate (33.2 mg, 0.40 mmol) and sodium ascorbate (19.2 mg, 0.10 mmol) were added to a solution of **(4)** (54.2 mg, 0.06 mmol) in $CHCl_3$ / MeOH (2:1, 24 mL). The solution was heated to 60 °C and stirred under an inert atmosphere of nitrogen with protection from light. The solvent was removed under reduced pressure, re-dissolved in CH_2Cl_2 (20 mL), and washed with H_2O (10 mL) and brine (10 mL). Organic extracts were combined and dried over Na_2SO_4, and the solvent was removed under reduced pressure to form a dark red/brown residue. Purification by silica gel column chromatography (gradient 100 % CH_2Cl_2 to 95 % CH_2Cl_2 / 5 % MeOH) formed the title compound as a dark red/brown solid (44.7 mg, 78 %). MALDI-MS (*m/z*): $[M]^+$ calcd. for $CH_{55}FeN_5O_7$, 941.34, found 941.3; UV-Vis ($CHCl_3$): λ_{max} / nm (ε / $M^{-1}cm^{-1}$) 382 (103265) *. *No extinction coefficient was recorded due to a broadening of the Q-bands.

Iron (II) 3,3'-(10-(4-(2-(ethyl(4-methyl-2-oxo-2*H*-chromen-7-yl) amino) ethoxy) phenyl)-3,7,8,12,13,17-hexamethylporphyrin-2,18-diyl) dipropionic acid, **AMC-Hem (6)**

Procedure adapted from Long and co-workers [13].

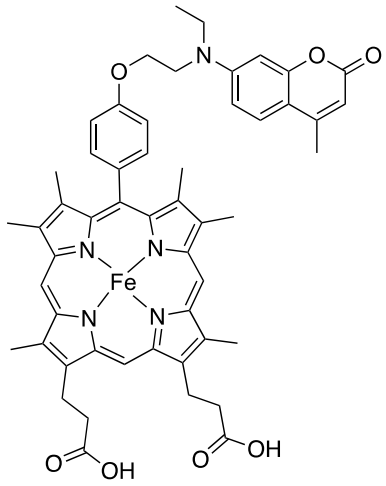

NaOH (4 M, 0.50 mL) was added to a solution of **AMC-Hem-porphyrin** (27.7 mg, 0.029 mmol) in CH_2Cl_2 (1 mL) and methanol (3 mL). The solution was heated to 40 °C and stirred under an inert atmosphere of nitrogen for 24 h. During the reaction, a dark red/brown precipitate appeared, indicating the formation of **AMC-Hem**. After 24 h the solvent was removed under reduced pressure to form a dark brown residue. The residue was re-dissolved in H_2O and acidified to pH 3-4 with HCl (12 M). The precipitate was isolated by centrifuge and washed with H_2O (20 mL) and CH_2Cl_2 (10 mL) and lyophilised to form the title compound as a dark purple/brown solid (24.6 mg, quant.). MALDI-MS (*m/z*): $[M]^+$ calcd. for $C_{52}H_{51}FeN_5O_7$, 913.31, found 913.31; HR-MS (m/z): $[M]^+$ calcd. for $C_{52}H_{51}FeN_5O_7$, 913.3132, found 913.3214; [UV-Vis ($CHCl_3$, λ_{max} / nm): (ε / $M^{-1}cm^{-1}$) 405 (100179), 504 (14248), 537 (8943), 571 (7123), 624 (3287).

Ethyl 4-(2-(ethyl(4-methyl-2-oxo-2*H*-chromen-7-yl)amino)ethoxy)benzoate **(7)**

Procedure adapted from Long and co-workers [13].

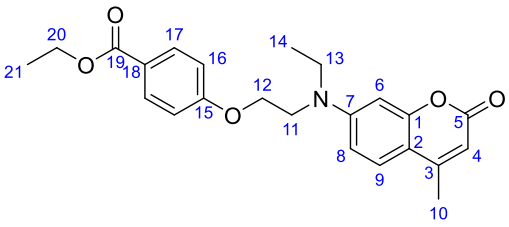

Ethyl 4-hydroxybenzoate (90 mg, 0.54 mmol) was added to a solution of K_2CO_3 (338 mg, 2.45 mmol) and KI (9 mg, 0.05 mmol) in dry acetonitrile (8 mL) and stirred at room temperature.7-((2-bromomethyl)(ethyl)amino)-4-methyl-2*H*-chromen-2-one (204 mg, 0.66 mmol) was subsequently added, and the reaction mixture was set to reflux at 82 °C for 22 h to give a pale-yellow solution. The resulting reaction mixture was diluted with DCM and filtered. The solution was then concentrated under reduced pressure and purification by silica gel column chromatography (gradient 100 % DCM to 80 % DCM / 20 % MeOH) to give the titled compound as a pale-yellow powder (100 mg, 38 %). ^{1}H NMR (400 MHz, $CDCl_3$): δ 7.94 – 7.89 (m, 2 H, H^{17}), 7.35 (d, 1 H, J = 9.0 Hz, H^9), 6.88 – 6.80 (m, 2 H, H^{16}), 6.62 (dd, 1 H, J_1 = 9.0 Hz, J_2 = 2.6 Hz, H^8), 6.51 (d, 1 H, J = 2.6 Hz, H^6), 5.89 (q, 1 H, J = 1.2 Hz, H^4), 4.27 (q, 2 H, J = 7.1 Hz, H^{20}), 4.15 (t, 2 H, J = 5.7 Hz, H^{12}), 3.75 (t, 2 H, J = 5.7 Hz, H^{11}), 3.49 (q, 2 H, J = 7.1 Hz, H^{13}), 2.28 (d, 3 H, J =

1.2 Hz, H^{10}), 1.31 (t, 3 H, J = 7.1 Hz, H^{21}), 1.19 (t, 3 H, J = 7.1 Hz, H^{14}); ^{13}C {^{1}H} NMR (101 MHz, $CDCl_3$): δ = 166.1 (C^{19}), 162.1 (C^{18}), 161.9 (C^{5}), 155.8 (C^{1}), 152.9 (C^{3}), 150.4 (C^{7}), 131.5 (C^{17}), 125.6 (C^{9}), 123.2 (C^{15}), 113.9 (C^{16}), 109.6 (C^{2}), 109.1 (C^{4}), 108.6 (C^{8}), 97.9 (C^{6}), 65.4 (C^{12}), 60.6 (C^{20}), 49.5 (C^{11}), 45.9 (C^{13}), 18.3 (C^{10}), 14.3 (C^{21}), 11.9 (C^{14}); HRMS (*m/z*): $[M+H]^+$ calcd. for $C_{23}H_{26}NO_5$, 396.1811, found 396.1804. UV-Vis ($CHCl_3$): λ_{max} / nm (ε / $M^{-1}cm^{-1}$) 364 (26012).

Methyl 4-(2-(ethyl(4-methyl-2-oxo-2*H*-chromen-7-yl)amino)ethoxy)benzoate **(8)**
Procedure adapted from Long and co-workers [13].

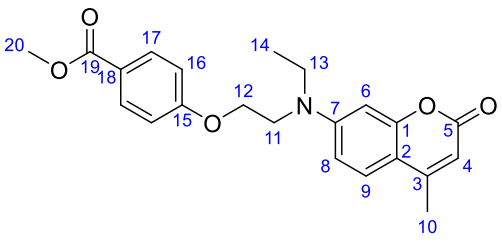

Methyl 4-hydroxybenzoate (188 mg, 1.23 mmol) was added to a solution of K_2CO_3 (355 mg, 2.57 mmol) and KI (85 mg, 0.51 mmol) in dry acetonitrile (8 mL) and stirred at room temperature. 7-((2-bromoethyl)(ethyl)amino)-4-methyl-2*H*-chromen-2-one (212 mg, 0.68 mmol) was subsequently added, and the resulting white solution was set to reflux at 82 °C for 18 h. The reaction mixture was then diluted with DCM and filtered. The solution was concentrated under reduced pressure and purification by silica gel column chromatography (gradient 100 % DCM to 80 % DCM / 20 % MeOH) formed the titled compound as a white crystalline powder (44 mg, 17 %). ^{1}H NMR (400 MHz, $CDCl_3$): δ = 7.97 (d, 2 H, J = 8.4 Hz, H^{17}), 7.40 (d, 1 H, J = 8.9 Hz, H^{9}), 6.88 (d, 2 H, J = 8.4 Hz, H^{16}), 6.69 – 6.62 (m, 1 H, H^{8}), 6.56 (s, 1 H, H^{6}), 5.96 (s, 1 H, H^{4}), 4.19 (t, 2 H, J = 5.7 Hz, H^{12}), 3.87 (s, 3 H, H^{20}), 3.80 (t, 2 H, J = 5.7 Hz, H^{11}), 3.54 (q, 2 H, J = 7.1 Hz, H^{13}), 2.34 (s, 3 H, H^{10}), 1.24 (t, 3 H, J = 7.1 Hz, H^{14}); ^{13}C {^{1}H} NMR (101 MHz, $CDCl_3$): δ = 166.8 (C^{19}), 162.3 (C^{18}), 162.1 (C^{5}), 156.0 (C^{1}), 152.9 (C^{3}), 150.5 (C^{7}), 131.8 (C^{17}), 125.8 (C^{9}), 123.2 (C^{15}), 114.1 (C^{16}), 109.9 (C^{2}), 109.5 (C^{4}), 108.7 (C^{8}), 98.3 (C^{6}), 65.5 (C^{12}), 52.0 (C^{20}), 49.8 (C^{11}), 46.2 (C^{13}), 18.6 (C^{10}), 12.2 (C^{14}); HRMS (*m/z*): $[M+H]^+$ calcd. for $C_{22}H_{24}NO_5$, 382.1654, found 382.1645. UV-Vis ($CHCl_3$): λ_{max} / nm (ε / $M^{-1}cm^{-1}$) 364 (22549).

4-(2-(ethyl(4-methyl-2-oxo-2*H*-chromen-7-yl)amino)ethoxy)benzoic acid **(9)**

Procedure adapted from Long and co-workers [13].

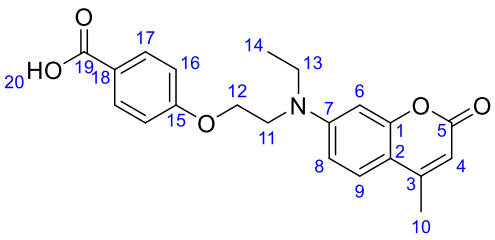

4M NaOH (0.47 mL) was added to a solution of **(7)** (53 mg, 0.13 mmol) in ethanol (3 mL) and set to reflux at 85 °C for 2 h. The reaction mixture was then cooled to room temperature before water (36 mL) was added, followed by the dropwise addition of 6M HCl until the pH reached ~ 1. The solution was concentrated under reduced pressure and purified by C18-reversed phase silica gel column chromatography (gradient 100 % water to 100 % acetonitrile) to give the titled compound an off-white solid (37 mg, 75 %). ^{1}H NMR (400 MHz, $(CD_3)_2SO$): δ = 12.71 (s, 1 H, H^{20}), 7.91 – 7.83 (m, 2 H, H^{17}), 7.51 (d, 1 H, J = 9.0 Hz, H^{9}), 7.04 – 6.96 (m, 2 H, H^{16}), 6.79 (dd, 1 H, J = 9.0 Hz, $^{4}J_{H\text{-}H}$ 2.5, H^{8}), 6.62 (d, 1 H, J = 2.4 Hz, H^{6}), 5.95 (s, 1 H, H^{4}), 4.22 (t, 2 H, J = 5.4 Hz, H^{12}), 3.82 (t, 2 H, J = 5.5 Hz, H^{11}), 3.54 (q, 2 H, J = 7.0 Hz, H^{13}), 2.32 (s, 3 H, H^{10}), 1.14 (t, 3 H, J = 6.9 Hz, H^{14}); ^{13}C {^{1}H} NMR (101 MHz, $(CD_3)_2SO$): δ = 167.0 (C^{19}), 162.0 (C^{18}), 160.8 (C^{5}), 155.5 (C^{1}), 153.6 (C^{2}), 150.7 (C^{7}), 131.4 (C^{17}), 126.2 (C^{9}), 123.2 (C^{15}), 114.3 (C^{16}), 108.9 (C^{8}), 108.8 (C^{4}), 108.1 (C^{3}), 97.3 (C^{6}), 65.8 (C^{12}), 48.9 (C^{11}), 45.1 (C^{13}), 18.0 (C^{10}), 11.9 (C^{14}); HRMS (*m/z*): $[M+H]^+$ calcd. for $C_{21}H_{22}NO_5$, 368.1498, found 368.1499. UV-Vis ($CHCl_3$): λ_{max} / nm (ε / $M^{-1}cm^{-1}$) 364 (8996).

Biological Methods

hMDM Isolation and cell culture

Human monocyte-derived macrophages (hMDMs) were isolated and cultured as previously described [15]. hMDMs were cultured in IMDM (Gibco catalogue #: 21056023) with 10% or 20% autologous human serum (AHS) and 1% Penicillin/Streptomycin (Gibco catalogue #: 15140122). 96-well black-sided clear bottom plates (Thermofisher catalogue #: 165305) were used for fluorescent cell-based or cell-free assays. hMDMs were plated at a density of 40,000 and 50,000 per well for enzyme activity and RT-qPCR, respectively. For RT-qPCR, cells were plated in 24-well plates (Sarstedt catalogue #: 83.3922). For live cell confocal microscopy, hMDMs were plated at a density of 100,000 cells per well.

Preparation of AHS

45 ml of blood was collected in sodium citrate vacutainers and centrifuged at 400 *xg* for 20 minutes at maximum acceleration and no brake. Afterwards, the plasma was collected and put into a universal container with 2% (v/v) $CaCl_2$ and a sterile broken glass Pasteur pipette to induce clotting.

Stimulation with hemin and pre-treatment with HDAC inhibitors

Unless otherwise stated, hMDMs were stimulated with 20 μM hemin (Sigma Catalogue #: H9039). hMDMs before stimulation were pre-incubated with each HDAC inhibitor for 1 hour at 10x the IC_{50} shown in **Supplementary Data 2 Table S1**. The catalogue numbers and suppliers of each HDAC inhibitor (HDACi) used in this study are shown in **Table S1.**

HDAC inhibitor	Supplier	Catalogue #
Trichostatin A	Apex Bio	A8183
Vorinostat	Apex Bio	A4084
Tucidinostat	Stratech	S8567
RGFP966	Apex Bio	A8803
Mocedinostat	Selleckchem	S1122
Panobinostat	Apex Bio	A8178
Tubacin	Apex Bio	A4501
TMP195	Apex Bio	A4183
PCI – 34051	Apex Bio	A4091
Santacruzamate A	Selleckchem	S7595

Table S1: Suppliers and catalogue numbers of the HDAC inhibits used in this study

Preparation of AMC-Hem

AMC-Hem was prepared as a black powder. Stock solutions of AMC-Hem were made in 100% DMSO (Sigma catalogue #: D2650). Sub-stocks of AMC-Hem for use with hMDMs were prepared in PBS or IMDM with a maximal volume-by-volume percentage of DMSO at 0.001%.

Analysis of AMC-Hem fluorescence

For each experiment with AMC-Hem, no probe controls for each condition were used. Subtracting values normalised the fluorescence intensity values in the wells with AMC-Hem from those without AMC-Hem. All fluorescent and absorbance measurements were taken using the BMG Labtech Clariostar^{Plus} microplate reader.

Oxidation and loading of red blood cells

Autologous red blood cells after separation from PBMCs were kept, and 5 ml was transferred to a 15 ml falcon tube. The 5 ml of autologous red blood cells was oxidised by adding 150 µl of 10 M hydrogen peroxide (Sigma Aldrich catalogue #:21,676-3) and left overnight (O/N) at 4ºC.

The OxRBCs were diluted 1:5 in PBS (Gibco catalogue #: 10010023) and incubated O/N with 100 µM AMC-Hem or 1 mM RuPPIX. After O/N incubation, the oxidised red blood cells (OxRBCs)) were washed with PBS and used to stimulate hMDMs. The OxRBCs were used at 10% (v/v) of the total well volume.

cDNA Synthesis and RT-qPCR

After stimulation, hMDMs were lysed in 300 µl Monarch RNA® Lysis buffer. RNA was extracted according to the instructions of the Monarch® Total RNA Miniprep Kit. cDNA was generated by adding 4 µl of LunaScript RT Supermix (NEB #E3010) to 20 µl of RNA and using the following protocol: 2 minutes at 25 °C, 10 minutes at 55 °C, and 1 minute at 95 °C. the cDNA was stored at -20 °C for future use.

RT-qPCR was performed by generating a master mix containing 5 µl Luna® Universal qPCR Master Mix (NEB catalogue #: M3033S), 0.25 µl forward primer, 0.25 µl reverse primer, and 2,5 µl of water. 8 µl of the master mix and 2 µl of sample cDNA was added per well. The qPCR reaction was run with following steps on a QuantStudio 6™: 2 minutes at 50 °C, 8 minutes at 95 °C, and 15 seconds at 95 °C followed by 1 minute at 61 °C repeated for 40 cycles.

RT-qPCR data are represented as fold change calculated by the delta delta Ct method [58].

Live cell hMDM confocal microscopy

hMDMs were cultured in 8-well chamber slides (Ibidi catalogue #: 80806) with the suspended lymphocytes for 48 h. After 48 h, the supernatant was removed and replaced with fresh media with 20% AHS. After incubation with AMC-Hem, the supernatant was removed and changed out for fresh media containing 10% AHS. The cells were then stained with 100 nM Syto13 (Invitrogen catalogue #: S7575) and 500 nM Lysotracker ™ Red DND-99 (Invitrogen catalogue #: L7528) for 1 h and then washed twice with fresh media containing 10% AHS. Cells were visualised on the Leica Stellaris STED Falcon, and images taken using the LAS X (Leica microsystems) software.

Immunofluorescence

After stimulation, the media was removed from the 8-well chamber slides, and the hMDMs were fixed in acetone for 5 – 10 minutes. The acetone was removed, and the slides were left to air-dry. Until staining, the chamber slides were stored at -80 ºC.

After defrosting, the wells were incubated with 10% normal goat serum for 1 h at room temperature to prevent non-specific goat anti-rabbit secondary antibody binding. Samples were stained in a pairwise fashion. Therefore, samples were stained with a mouse monoclonal against 1:1000 lysosome-membrane-associated protein 1 (LAMP1) (Abcam catalogue #: ab302639) and either a rabbit monoclonal against 1:500 HO-1 (Abcam catalogue #: ab52947 or 1:200 CYP450POR (Abcam catalogue #: ab180597). Samples were also stained with a mouse monoclonal against 1:200 glucose-6-phosphate dehydrogenase conjugated (G6PD) to AlexaFluor488 (Proteintech catalogue #: CL488-66373) and either a rabbit monoclonal against HO-1 or CYP450POR, as previously stated. Primary antibody staining was performed O/N at 4ºC

After O/N incubation, the wells were washed three times with PBS and incubated with a goat anti-rabbit secondary antibody conjugated to AlexaFluor647 (Invitrogen Catalogue #: A-21245) at 1:200 for 2 h at room temperature. Primary unconjugated mouse monoclonal antibodies were detected by incubation with a goat anti-mouse secondary antibody conjugated to AlexaFluor488 (Abcam Catalogue #: ab150113) at 1:200 for 2 h at room temperature. After 2 h, the wells were washed with PBS three times and counterstained with 100 nM Sytox Orange (Invitrogen catalogue #: S11368) for 10 minutes. The wells were washed three times again and 200 µl of an 80/20% PBS-Glycerol solution was added to each well and visualised. All images were visualised on the Leica Stellaris STED Falcon and images were taken using the LAS X (Leica microsystems) software.

Image Analysis

All images were analysed using Fiji (NIH, Bethesda) and custom macros provided Mr. Stephen Rothery. Unless otherwise indicated, all 2D images were generated using the "enhanced gallery" macro. The fluorescent intensity in each channel was determined by selecting a region of interest (ROI) and applying the multi-measure tool. The mean intensity column was selected and used. For statistical analysis, mean intensities from 20 cells per biological replicate were averaged to generate a grand mean. The grand mean per condition was normalised against the grand mean intensity of the control cells.

Quantification of the fluorescence intensity at different radial distances in the AMC-Hem and lysotracker channel was performed using the radial measures tool macro (**Figure 1 Arrow 1)**. A single cell was chosen as an ROI, the centre of the lysosome was chosen as the centre point, and radii were automatically created at 45 degrees (**Figure 1 Arrow 2 and 3**). This creates 8 lines per ROI. Per cell, the list function was used to obtain the raw pixel intensities at each distance and transferred to Excel for further analysis (**Figure 1 Arrow 4**). These values were imported into Excel, distance values rounded to the nearest integer, and a pivot table was generated to determine the average pixel value per integer distance value. Per biological replicate, this was repeated for three cells and the average intensity at each distance was used for statistical analysis.

Pixel values for line ROIs were determined using the custom macro "Multi Line Intensity Profiles for a time series". These values were imported into Excel, distance values rounded to the nearest integer, and a pivot table was generated to determine the average pixel value per integer distance value.

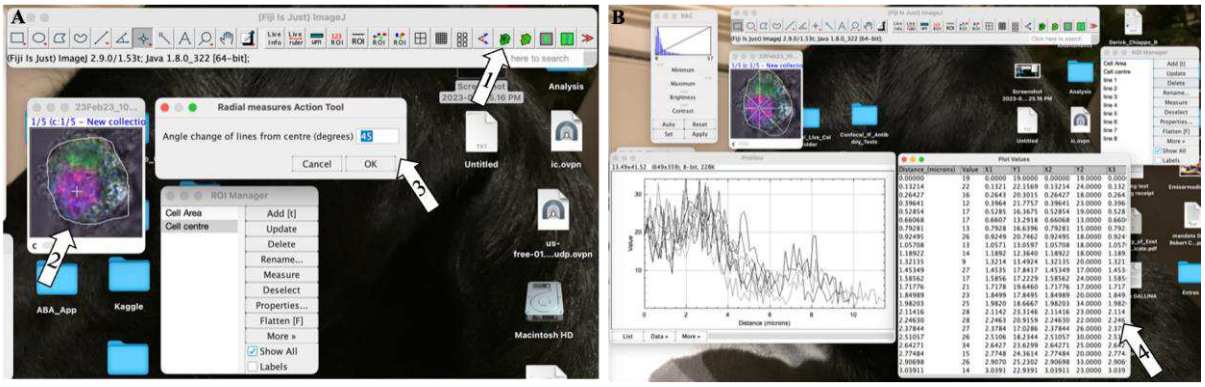

Figure 1: Radial measure tool macro

Preparation of murine S9 fraction

Historically collected mouse livers were thawed and homogenised using a polytron PT-1300 D handheld homogeniser at 4 ºC in 50 mM Tris-HCL, 2 mM EDTA, and 150 mM KCL. The homogenate was transferred into 1.5 ml Eppendorf and was centrifuged at 16,000 *xg* for 25 minutes at 4 ºC. The supernatant was collected, transferred to a new Eppendorf, and stored at -20 ºC for future use.

Serum HO-1 activity

Before optimisation, serum HO-1 activity was measured in a 100 µl solution with 100% serum, 0.2 mM NADPH (Merck Millipore catalogue #: 481973), and 5 µM AMC-Hem. Emission measurements were taken daily for 96 h. Post optimisation, an assay buffer composed of 10% (v/v) serum, 2 mM glucose-6-phosphate (Merck Millipore catalogue #: 10127647001), 0.17 units glucose-6-phosphate dehydrogenase (Sigma-Aldrich catalogue #: G7877), 1 mM NADP+ (Merck Millipore catalogue #: 481972), 1 mM NADPH, and 12% (v/v) murine liver S9 fraction (**Table S2**). Emission measurements were taken every 15 minutes for 2 h at 37 ºC. Data was processed as described in the "**Analysis of AMC-Hem fluorescence**" section of the methods.

Component	Reagent (units)	Amount used
Sample	Serum (%, v/v)	10
NADPH-generating System		
	Glucose-6-phosphate (mM)	2
	Glucose-6-phosphate dehydrogenase (units)	0.17
	NADP+ (mM)	1
Electron Source		
	NADPH (mM)	1
	Murine liver S9 fraction (%, v/v)	12

Table S2: Composition of serum assay buffer post-optimisation

HO-1 ELISA

Serum levels of HO-1 were assayed using a commercial ELISA (RD Systems catalogue #: DYC3776-5) per the manufacturer's instruction.

Serum HO-1 kcat calculations

The k_{cat} or turnover number for serum HO-1 was calculated by first generating a standard curve using AMC-Hem breakaway product with the following concentrations (μM): 10,3,1,0.03,0.01, and 0. A line of best fit was generated and used to convert normalized fluorescence to μM of AMC-Hem breakaway product. The k_{cat} was then calculated by dividing picomoles of AMC-Hem breakaway product/time divided by picomoles of HO-1 enzyme.

Statistical analysis

Data were analysed and visualized in Prism. All data were tested for normality using the Shapiro-Wilk's test. Two-group parametric data and non-parametric data was tested by Student's t-test or Wilcoxon-Mann-Whitney, respectively. Multiple group parametric data was tested by one-way analysis of variance (ANOVA) with Bonferroni's correction. Multiple group non-parametric data was tested by ANOVA with Holm-Sidak posthoc testing.

References

[1] Kawashima A, Oda Y, Yachie A, et al. Heme oxygenase–1 deficiency: The first autopsy case. *Hum Pathol* 2002; 33: 125–130.

[2] Radhakrishnan N, Yadav SP, Sachdeva A, et al. Human Heme Oxygenase-1 Deficiency Presenting with Hemolysis, Bleeding, Nephritis, Asplenia and Inflammation. *Blood* 2009; 114: 3013.

[3] Poss KD, Tonegawa S. Heme oxygenase 1 is required for mammalian iron reutilization. *Proc Natl Acad Sci U S A* 1997; 94: 10919–10924.

[4] Boyle JJ. Heme and haemoglobin direct macrophage Mhem phenotype and counter foam cell formation in areas of intraplaque haemorrhage. *Curr Opin Lipidol* 2012; 23: 453.

[5] Frostegård J. Immunity, atherosclerosis and cardiovascular disease. *BMC Med* 2013; 11: 117.

[6] Michel J-B, Martin-Ventura JL, Nicoletti A, et al. Pathology of human plaque vulnerability: mechanisms and consequences of intraplaque haemorrhages. *Atherosclerosis* 2014; 234: 311–319.

[7] Walter ERH, Cooper SM, Boyle JJ, et al. Enzyme-activated probes in optical imaging: a focus on atherosclerosis. *Dalton Trans* 2021; 50: 14486–14497.

[8] Boyle JJ, Harrington HA, Piper E, et al. Coronary intraplaque hemorrhage evokes a novel atheroprotective macrophage phenotype. *Am J Pathol* 2009; 174: 1097–1108.

[9] Wan X, Huo Y, Johns M, et al. 5'-AMP-activated protein kinase-activating transcription factor 1 cascade modulates human monocyte-derived macrophages to atheroprotective functions in response to heme or metformin. *Arterioscler Thromb Vasc Biol* 2013; 33: 2470–2480.

[10] Seneviratne A, Han Y, Wong E, et al. Hematoma Resolution In Vivo Is Directed by Activating Transcription Factor 1. *Circ Res* 2020; 127: 928–944.

[11] True AL, Olive M, Boehm M, et al. Heme Oxygenase-1 Deficiency Accelerates Formation of Arterial Thrombosis Through Oxidative Damage to the Endothelium, Which Is Rescued by Inhaled Carbon Monoxide. *Circ Res* 2007; 101: 893–901.

[12] Poss KD, Tonegawa S. Reduced stress defense in heme oxygenase 1-deficient cells. *Proc Natl Acad Sci U S A* 1997; 94: 10925–10930.

[13] Walter ERH, Ge Y, Mason JC, et al. A Coumarin–Porphyrin FRET Break-Apart Probe for Heme Oxygenase-1. *J Am Chem Soc* 2021; 143: 6460–6469.

[14] Mostovnikov VA, Rubinov AN, Anufrik SS, et al. Effect of the molecular structure of coumarin derivatives on the spectral-luminescent and generating properties of their solutions. *J Appl Spectrosc* 1977; 27: 866–871.

[15] Boyle JJ, Johns M, Kampfer T, et al. Activating Transcription Factor 1 Directs Mhem Atheroprotective Macrophages Through Coordinated Iron Handling and Foam Cell Protection. *Circ Res* 2012; 110: 20–33.

[16] Roman G, Riley JG, Vlahakis JZ, et al. Heme oxygenase inhibition by 2-oxy-substituted 1-(1H-imidazol-1-yl)-4-phenylbutanes: Effect of halogen substitution in the phenyl ring. *Bioorg Med Chem* 2007; 15: 3225–3234.

[17] Alaoui-Jamali MA, Bismar TA, Gupta A, et al. A Novel Experimental Heme Oxygenase-1–Targeted Therapy for Hormone-Refractory Prostate Cancer. *Cancer Res* 2009; 69: 8017–8024.

[18] Ning Z-Q, Li Z-B, Newman MJ, et al. Chidamide (CS055/HBI-8000): a new histone deacetylase inhibitor of the benzamide class with antitumor activity and the ability to enhance immune cell-mediated tumor cell cytotoxicity. *Cancer Chemother Pharmacol* 2012; 69: 901–909.

[19] Negmeldin AT, Padige G, Bieliauskas AV, et al. Structural Requirements of HDAC Inhibitors: SAHA Analogues Modified at the C2 Position Display HDAC6/8 Selectivity. *ACS Med Chem Lett* 2017; 8: 281–286.

[20] Malvaez M, McQuown SC, Rogge GA, et al. HDAC3-selective inhibitor enhances extinction of cocaine-seeking behavior in a persistent manner. *Proc Natl Acad Sci U S A* 2013; 110: 2647–2652.

[21] Hoeksema MA, Gijbels MJ, Van den Bossche J, et al. Targeting macrophage Histone deacetylase 3 stabilizes atherosclerotic lesions. *EMBO Mol Med* 2014; 6: 1124–1132.

[22] Pavlik CM, Wong CYB, Ononye S, et al. Santacruzamate A, a Potent and Selective Histone Deacetylase (HDAC) Inhibitor from the Panamanian Marine Cyanobacterium cf. Symploca sp. *J Nat Prod* 2013; 76: 10.1021/np400198r.

[23] Tenhunen R, Marver HS, Schmid R. The enzymatic conversion of heme to bilirubin by microsomal heme oxygenase. *Proc Natl Acad Sci U S A* 1968; 61: 748–755.

[24] Tenhunen R, Marver HS, Schmid R. Microsomal heme oxygenase. Characterization of the enzyme. *J Biol Chem* 1969; 244: 6388–6394.

[25] McNally SJ, Ross JA, James Garden O, et al. Optimization of the paired enzyme assay for heme oxygenase activity. *Anal Biochem* 2004; 332: 398–400.

[26] Sarpong-Kumankomah S, Gailer J. Identification of a haptoglobin-hemoglobin complex in human blood plasma. *J Inorg Biochem* 2019; 201: 110802.

[27] LysoTracker™ Red DND-99, special packaging, https://www.thermofisher.com/order/catalog/product/L7528 (accessed 24 July 2023).

[28] Klei TRL, Meinderts SM, van den Berg TK, et al. From the Cradle to the Grave: The Role of Macrophages in Erythropoiesis and Erythrophagocytosis. *Front Immunol*; 8, https://www.frontiersin.org/articles/10.3389/fimmu.2017.00073 (2017, accessed 14 August 2023).

[29] Michel J-B, Virmani R, Arbustini E, et al. Intraplaque haemorrhages as the trigger of plaque vulnerability. *Eur Heart J* 2011; 32: 1977–1985.

[30] Kovtunovych G, Eckhaus MA, Ghosh MC, et al. Dysfunction of the heme recycling system in heme oxygenase 1–deficient mice: effects on macrophage viability and tissue iron distribution. *Blood* 2010; 116: 6054–6062.

[31] Sugishima M, Sato H, Higashimoto Y, et al. Structural basis for the electron transfer from an open form of NADPH-cytochrome P450 oxidoreductase to heme oxygenase. *Proc Natl Acad Sci* 2014; 111: 2524–2529.

[32] Bories GFP, Yeudall S, Serbulea V, et al. Macrophage metabolic adaptation to heme detoxification involves CO-dependent activation of the pentose phosphate pathway. *Blood* 2020; 136: 1535–1548.

[33] Tenhunen R, Marver HS, Schmid R. The enzymatic conversion of heme to bilirubin by microsomal heme oxygenase. *Proc Natl Acad Sci U S A* 1968; 61: 748–755.

[34] Delaby C, Rondeau C, Pouzet C, et al. Subcellular Localization of Iron and Heme Metabolism Related Proteins at Early Stages of Erythrophagocytosis. *PLOS ONE* 2012; 7: e42199.

[35] Santarino IB, Vieira OV. Maturation of phagosomes containing different erythrophagocytic particles in primary macrophages. *FEBS Open Bio* 2017; 7: 1281–1290.

[36] Li X, Li C, Hou L, et al. Higher Level of Serum Heme Oxygenase-1 in Patients With Intracerebral Hemorrhage. *Int Surg* 2015; 100: 1220–1224.

[37] Idriss NK, Lip GYH, Balakrishnan B, et al. Plasma haemoxygenase-1 in coronary artery disease. A comparison with angiogenin, matrix metalloproteinase-9, tissue inhibitor of metalloproteinase-1 and vascular endothelial growth factor. *Thromb Haemost* 2010; 104: 1029–1037.

[38] Tang D, Tang W-J, Shi X-L, et al. Association of the microsatellite (GT)n repeat polymorphisms of the HO-1 gene promoter and corresponding serum levels with the risk of laryngeal squamous cell carcinoma. *Acta Otolaryngol (Stockh)* 2016; 136: 806–811.

[39] Kirino Y, Takeno M, Iwasaki M, et al. Increased serum HO-1 in hemophagocytic syndrome and adult-onset Still's disease: use in the differential diagnosis of hyperferritinemia. *Arthritis Res Ther* 2005; 7: R616.

[40] Telford W, Stickland L, Koschorreck M. Ultraviolet 320 nm Laser Excitation for Flow Cytometry. *Cytom Part J Int Soc Anal Cytol* 2017; 91: 314–325.

[41] Telford WG. Overview of Lasers for Flow Cytometry. In: Hawley TS, Hawley RG (eds) *Flow Cytometry Protocols*. New York, NY: Springer, pp. 447–479.

[42] Nakamichi I, Habtezion A, Zhong B, et al. Hemin-activated macrophages home to the pancreas and protect from acute pancreatitis via heme oxygenase-1 induction. *J Clin Invest* 2005; 115: 3007–3014.

[43] Collino M, Pini A, Mugelli N, et al. Beneficial effect of prolonged heme oxygenase 1 activation in a rat model of chronic heart failure. *Dis Model Mech* 2013; 6: 1012–1020.

[44] Huber WJ, Backes WL. Expression and characterization of full-length human heme oxygenase-1: the presence of intact membrane-binding region leads to increased binding affinity for NADPH cytochrome P450 reductase. *Biochemistry* 2007; 46: 12212–12219.

[45] Huber WJ, Marohnic CC, Peters M, et al. Measurement of membrane-bound human heme oxygenase-1 activity using a chemically defined assay system. *Drug Metab Dispos Biol Fate Chem* 2009; 37: 857–864.

[46] Connick JP, Reed JR, Cawley GF, et al. Heteromeric complex formation between human cytochrome P450 CYP1A1 and heme oxygenase-1. *Biochem J* 2021; 478: 377–388.

[47] Sambrano GR, Parthasarathy S, Steinberg D. Recognition of oxidatively damaged erythrocytes by a macrophage receptor with specificity for oxidized low density lipoprotein. *Proc Natl Acad Sci U S A* 1994; 91: 3265–3269.

[48] Setsukinai K, Urano Y, Kakinuma K, et al. Development of novel fluorescence probes that can reliably detect reactive oxygen species and distinguish specific species. *J Biol Chem* 2003; 278: 3170–3175.

[49] Zhang Q, Zhao K, Shen Q, et al. Tet2 is required to resolve inflammation by recruiting Hdac2 to specifically repress IL-6. *Nature* 2015; 525: 389–393.

[50] Wu C, Li A, Hu J, et al. Histone deacetylase 2 is essential for LPS-induced inflammatory responses in macrophages. *Immunol Cell Biol* 2019; 97: 72–84.

[51] Darbari DS, Sheehan VA, Ballas SK. The vaso-occlusive pain crisis in sickle cell disease: Definition, pathophysiology, and management. *Eur J Haematol* 2020; 105: 237–246.

[52] Basu M, Saha S, Ukil A. Spectrophotometric Assessment of Heme Oxygenase-1 Activity in Leishmania-infected Macrophages. *Bio-Protoc* 2020; 10: e3578.

[53] Chen F, Zhang B, Ding Z, et al. Hemin as a General Static Dark Quencher for Constructing Heme Oxygenase-1 Fluorescent Probes. *Angew Chem Int Ed Engl* 2023; 62: e202301598.

[54] Fields GB. Using fluorogenic peptide substrates to assay matrix metalloproteinases. *Methods Mol Biol Clifton NJ* 2001; 151: 495–518.

[55] Gelsthorpe AR, Wells RS, Lowe AP, et al. High-throughput class I HLA genotyping using fluorescence resonance energy transfer (FRET) probes and sequence-specific primer-polymerase chain reaction (SSP-PCR). *Tissue Antigens* 1999; 54: 603–614.

[56] Xu X, Gerard AL, Huang BC, et al. Detection of programmed cell death using fluorescence energy transfer. *Nucleic Acids Res* 1998; 26: 2034–2035.

[57] Lin Q, Bao C, Cheng S, et al. Target-Activated Coumarin Phototriggers Specifically Switch on Fluorescence and Photocleavage upon Bonding to Thiol-Bearing Protein. *J Am Chem Soc* 2012; 134: 5052–5055.

[58] Livak KJ, Schmittgen TD. Analysis of relative gene expression data using real-time quantitative PCR and the 2(-Delta Delta C(T)) Method. *Methods San Diego Calif* 2001; 25: 402–408.